International Journal of Multiphase Flow 104 (2018) 322–337

Contents lists available at ScienceDirect

International Journal of Multiphase Flow

journal homepage: www.elsevier.com/locate/ijmulflow

Review

Status and future developments of Large-Eddy Simulation of turbulent multi-fluid flows (LEIS and LESS)

Djamel Lakehal

ASCOMP AG, Zürich, Switzerland

ARTICLE INFO

Article history:
Received 6 July 2017
Revised 14 February 2018
Accepted 22 February 2018
Available online 7 March 2018

Keywords:
LES
LEIS
LESS
Multi-fluid flow
ITM
Phase averaging/filtering

ABSTRACT

Current computational trends related to turbulent gas-liquid flow are discussed, together with the developments and open challenges needed to bring the discipline to a mature stage. The contribution presents the possibilities offered today by turbulent scale-resolving strategies (Large-Eddy Simulation, LES) to treat complex, multiphase flow topology in system components, and transcending more conventional kinetic energy dissipation-based models combined with phase-average approaches. The LES approach of turbulent gas-liquid flows introduced here under its sub-variants LESS and LEIS (Large-Eddy & Structures Simulation and Large-Eddy & Interface Simulation) is based on unifying the phase averaging concept and the turbulent-scale filtering operations into one single process. The paper is written in the spirit of a review, albeit it provides enough derivation details including the connection between the supergrid (resolved) and subgrid (unresolved) physics. A particular attention is paid here to the various attempts to model the underlying subgrid physics, including DNS-based model upscaling. A brief review of LEIS and LESS applications to phase-change heat transfer problems is provided, too. While the LESS variant based on the filtered multi-fluid equations is best suited for a range of problems in which one of the phases is dispersed in the other, LEIS provides further accuracy by directly predicting interface dynamics and turbulence motions down to the grid level. The paper addresses also the required developments for more complex multi-scale, multi-fluid flow problems, including a new approach termed as ARM, short for All-Regime Multiphase flow model.

1. Introduction

The computational multi-fluid flow scene has gone through successive transitions motivated by new, sometimes challenging needs and developments. The first real transition triggered in the 1980s focused on gradually removing the limitations of lumped-parameter 1D modeling (used essentially in the oil and gas and nuclear energy sectors) by further developing the phase-average approach (homogeneous and two-fluid models) for 3D turbulent flow problems. This is now state-of-the-art. The advent of the so-called Interface Tracking Methods (ITM) in the late 80s (Kataoka, 1986), which permit to better predict the shape of interfaces while minimizing the modeling assumptions, has somewhat shifted the interest towards a new era, known today as CMFD, short for Computational Multi-Fluid Dynamics. The most recent transition is now underway: it specifically centers on the use of these new simulation techniques (ITM) for practical, turbulent flow problems present in the energy and processes segment. This latest transition initiated in the 2000s has been marked by the gradual migration from the phase-average formulation to more refined interface tracking methods (ITMs), and from statistical Reynolds averaged modeling (RANS) to scale-resolving turbulence simulation including Large-Eddy Simulation (LES) and its sub-variants: dispersed-flow LES referred to here as LESS, short for Large-Eddy and Structure Simulation, and Interfacial-flow LES baptized LEIS (Lakehal, 2010), short for Large-Eddy and Interface Simulation. The migration was essentially motivated by the weaknesses of phase averaging to predict various (sometimes rather simple) types of topologies, e.g. stratifying slug flow, and also because statistical turbulence modeling is of limited predictive performance in the multiphase flow context. As it will be thoroughly discussed in this paper, the extensive investigation devoted to extending LES to multiphase gas-liquid flows raised specific questions as to the modeling of the unresolved flow physics, e.g. the contribution of the unresolved dispersed phase to the dissipation mechanism in LESS (Vaidheeswaran and Hibiki, 2017), and the asymptotic behavior of turbulence at the interface in LEIS (Reboux et al., 2006). These were central for the LESS and LEIS concepts and have to some extent benefited from DNS (Fulgosi et al., 2003; Tabib and Schwarz, 2011) and detailed experiments for model upscaling (Simiano et al., 2009), albeit not at the

E-mail address: lakehal@ascomp.ch

https://doi.org/10.1016/j.ijmultiphaseflow.2018.02.018
0301-9322/

same extent as what has been learnt from DNS of particle-laden flows (Elghobashi and Truesdell, 1993; Ferrante and Elghobashi, 2003).

LESS has been employed under the two-fluid and mixture model variants essentially for turbulent bubbly flows (Deen et al., 2001; Milelli et al., 2001; Lakehal et al., 2002; Lakehal, 2004). Other contributions appeared subsequently in the literature, using some form of LESS for a variety of dispersed gas liquid flows (Ničeno et al., 2008; Capecelatro and Desjardins, 2013; Ma et al., 2016; Yang et al., 2016). The derivation of the LESS equations can be found in the papers of Lakehal et al. (2002) and Sirignano (2005); the latter considered heat transfer and chemical reaction, too. LEIS has been applied to turbulent gas-liquid flows involving large-scale sheared interfaces, with problems ranging from spilling wave flows (Lakehal and Liovic, 2011) to steam injection in a water pool (Li et al., 2015). Lately, Lakehal et al. (2017) simulated a turbulent channel flow laden with resolved bubbles clustered near the wall. But the progress in hardware technology is helping LEIS gain in popularity in the jet-atomization community in particular (Buonfiglioli and Mendonça, 2005; Desjardins et al., 2010; Chesnel et al., 2011; Duret et al., 2013; Kaario et al., 2013; Jarrahbashi and Sirignano, 2014; Navarro-Martinez, 2014; Behzad et al., 2016; Hélie et al., 2016). LEIS is indeed capable of predicting primary breakup without necessarily introducing additional sub-grid scale models, which could be required for secondary breakup mechanisms (Klein et al., 2015). Full DNS of liquid jet primary and secondary breakup indeed requires massive mesh resolutions (Shinjo and Umemura, 2010).

We proceed by posing the issue of scale segregation in multi-fluid flows to make the analogy with conventional LES clear. In the second part we review the extension of LES to multi-fluid gas-liquid flows, from early-to-mid 2000s where the fundamentals of LES of gas-liquid flows was published for the first time, until the very recent developments in terms of model upscaling and novel predictive strategies. We then aboard the wide spectrum of multi-fluid flow modeling routes, from the microscopic description up to resolved-scale and unresolved-scale strategies. We then review past work on the derivation of each approach, from the concept of filtering to subgrid-scale modeling. Finally we discuss developments underway as to unifying the two approaches towards what we refer to as ARM, short for All-Regime Multiphase flow model. The paper does not address the use of LES for particle laden flows; a review is dedicated to the subject by Fox (2012).

2. Turbulent multi-fluid flows

2.1. Scale segregation

The notion of 'flow scales' in turbulent multi-fluid flow systems needs to be clarified prior to invoking computational techniques and models. To illustrate this notion, we proceed by analyzing the wave breaking flow depicted in Fig. 1 to which we could look at as a combination of turbulence scales interacting with the topology or interfacial scales. Here the interfacial sublayer is substantially sheared and interacts with the free surface causing intermittent high and low curvature areas. To what extent this phenomenon can be affected by the underlying turbulence is not clear, however, what matters when it comes to prediction is to avoid smoothing out interface deformations and turbulence structures. The flow regime evolves gradually from stratified with capillary waves to large-scale waves by the action of pressure and gas-shear by extracting kinetic energy from the mean flow; it ultimately breaks into small scales and dissipates its energy. Interfacial scales range therefore from the size of individual droplets/bubbles to the wave slope.

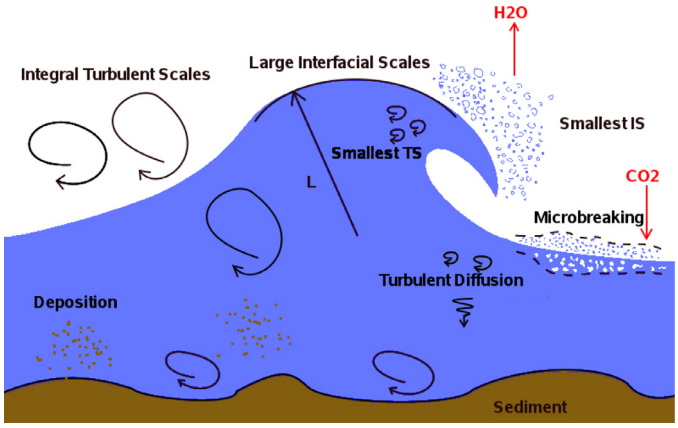

Fig. 1. Breaking wave flow.

Turbulence is generated at the interface by friction and subsequent to wave plunging (in addition to inflow and wall turbulence). The hydrodynamic instability caused by the shear between two adjacent flows is in effect a transition to turbulence and can be a major source of turbulence. A cascade process with the generation of smaller length scales occurs, until capillary action prevails. The spectrum of turbulence varies depending on the imposed flow conditions, ranging from low-frequency integral scales to high-frequency scales developing at the crest of the wave, near breaking. Dispersed droplets and bubbles created by wave entrainment and spilling - generating surface foam - disperse by reaction to turbulence. The picture is complete; it needs now to be translated in terms of modeling and simulation principles. The flow scenario discussed above requires tailored computational methods since it presents various facets in terms of topology: the dispersed mixed flow regions can only be treated using a phase-averaged formulation since the scales are unresolvable on typical CFD grids, while wave deformations can be simulated using ITM's since the interface is sufficiently large to be resolved in a typical grid.

2.2. Scale-resolving strategies

Considering topology changes, ITM's are best suited to locate the interface, not by following it in a Lagrangian sense, but by keeping track of its topology in an Eulerian sense through the evolution of an appropriate phase-indicator field or color function. Examples include the Level-Set method (Osher and Sethian, 1988) in which the interface is considered to be a level surface of a function that is defined over all space, and the VOF method (Hirt and Nichols, 1981), in which the location of the interface is captured by keeping track of the volume fraction of each computational cell in the grid with respect to one of the fluid phases. Phase-average process is in essence a filtering process since the portion of the spectrum associated with smaller interfacial scales is filtered out: it can thus be applied to treat mixed flows containing a dispersed phase whose exact topology is otherwise unresolvable on Eulerian grids, and can be performed under different forms, including multi-realization ensemble averaging, volume averaging, etc. As to turbulence, the big-picture distinguishes between (i) turbulence-scale resolving methods, including DNS (all the scales), LES (larger scales than the grid-imposed filter) and its sub-scale variants like Very-Large Eddy Simulation and Detached Eddy Simulation (V-LES and DES), and statistical time averaging based on the Reynolds averaged Navier–Stokes equations (RANS).

Clearly, modeling a specific flow involving a combination of topology and turbulence length scales requires combining specific computational techniques with selected models to cope with the

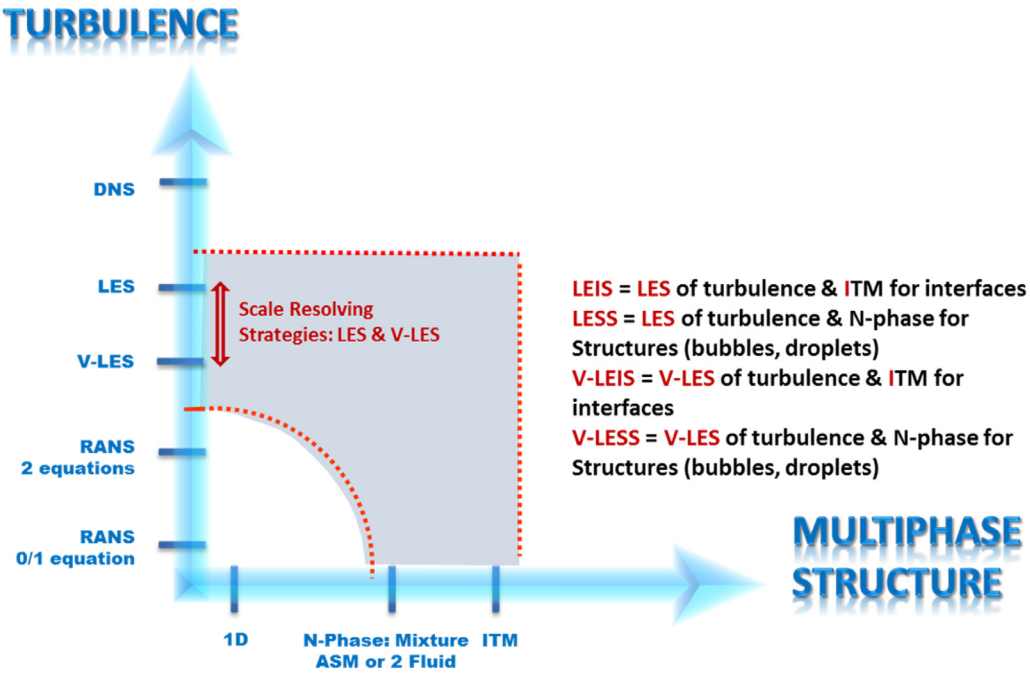

Fig. 2. Possible combinations of computational techniques and models.

underlying physics, as shown in Fig. 2. Because in LES the grid size is related to the smallest resolvable turbulence length scale, it can be straightforwardly combined with any ITM in which the smallest resolvable scale is of the order of the grid cell as well. The combination of the two brings a notable advantage, that is: besides delivering the time-dependent interfacial kinematics, the need to model the interfacial exchange terms is alleviated. Combining V-LES where the filter width is larger than the grid size is also possible with ITM's (Labois and Lakehal, 2011).

What is conflicting though is to work with the RANS/ITM combination, unless the interface motion is too slow and almost flat, in other words, when the target 'figure of merit' is not the grid-scale surface curvature for ITM. Still, in both contexts, sub-grid scales effects are still needed to be modeled. While the LES of interfacial flows can only be achieved in the context of Interface Tracking, the LES of dispersed two-phase flows can only be performed in the phase average, multi-fluid flow framework, as a 'filtering' process. The question is how phase averaging and LES turbulent-scale filtering operations can be combined into one single process.

2.3. From phase averaging to phase filtering

Volume averaging was first used within the combustion modeling community dealing with spray systems (Crocco and Cheng, 1956; Williams, 1962); the book of Sirignano (1999) is a very good reference for the work done in that context, until that time. Later on, the volume averaging strategy has been adopted by Whitaker (1966, 1967) and Slattery (1967) for the modeling of flows in porous media. Bataille (1981) generalized the approach for laminar two-phase flow in connection with the multi-fluid flow context. Bataille's (1981) derivation made a clear distinction between filtering and volume averaging by introducing for the first time a weight function in the convolution product, which has until then been systematically taken as equal to unity. For turbulent, variable-density flows, known advances have been essentially made in the combustion area, where filtering of the transport equations (including that of the flame propagation) is a common practice (Im et al., 1997). The first contributions introducing the derivation of the filtered multi-fluid flow equations under isothermal flow conditions were due to Lakehal et al. (2002) and shortly after to Sirignano (2005), who has generalized the strategy to further cope with reactive flows. Both contributions propose an extension of filtering for turbulent flows to combine interfacial and turbulence scales into one unified filter. The filtered Single-fluid flow equations were subsequently derived by Lakehal (2004) and Liovic and Lakehal (2007, 2006), at the same time as Labourasse et al. (2007). The strategy has since then been widely adopted in the combustion modeling community dealing with jet atomization in particular, as presented in the Introduction.

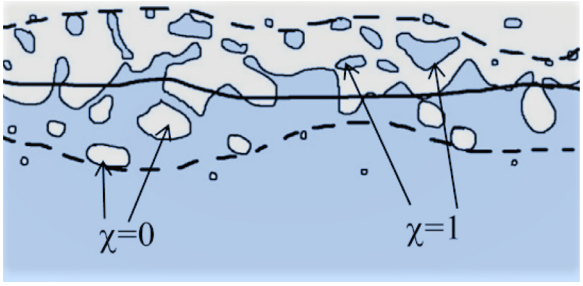

Fig. 3. Phase indicator functions in generic multi-fluid flow systems.

3. Multi-fluid flow modeling

3.1. Microscopic description

We proceed by considering a multi-fluid system occupied by two fluid species of density ρ^k and dynamic viscosity μ^k, illustrated in Fig. 3. For simplicity, we restrict the introduction to the case of liquid and gas, indicated henceforth by $k = L$ and $k = G$. The liquid phase is the continuous media, whereas the gas phase (also continuum) is present either in form of N distinct structures (e.g. bubbles or droplets), or as a separate phase in direct contact with the liquid. To distinguish fluid volumes within the entire domain, a phase indicator (or distribution) function (Lance et al., 1979) is

defined, such that (Fig. 3):

$$\chi^k(\mathbf{x},t) = \begin{cases} 1 & for \;\; \mathbf{x} \in phase\; k \\ 0 & otherwise \end{cases} \tag{1}$$

This is obviously similar to the intermittency function ξ used in turbulence for conditional averaging, where

$$\xi^k(\mathbf{x},t) = \begin{cases} 1 & for \;\; \mathbf{x} \in turbulent\, field \\ 0 & otherwise \end{cases} \tag{2}$$

The function was earlier introduced as a void-volume-distribution function in the '60s by the porous-media community (Whitaker, 1966; 1967; Slattery, 1967) for volume averaging over the micro- structure that included both the solid porous material and the fluid in the pores. In the present context, the function has a different meaning, depending on the way the transport equations are interpreted after averaging. It may refer to a probability of phase presence (or absence), as it may designate a space distribution function. The gradient of the phase indicator function and the surface curvature (κ) are defined by,

$$\nabla\chi^k = -\mathbf{n}^k\delta(\mathbf{x}-\mathbf{x}_I), \quad \kappa = -\nabla\cdot\mathbf{n} \tag{3}$$

where $\mathbf{n}^k = \nabla\chi^k/|\nabla\chi^k|$ is the normal unit vector pointing outward of phase k (with $\mathbf{n^L} = -\mathbf{n^G} \equiv \mathbf{n}$), and δ is the Dirac function marking the interface location with $\mathbf{x}_I$. Lagrangian invariance applies for $\chi^k(\mathbf{x}, t)$, reflecting its passive advection with the flow by the topological equation (Drew and Passman, 1999):

$$\frac{\partial\chi^k}{\partial t} + \mathbf{u}_I\cdot\nabla\chi^k = 0, \tag{4}$$

which we could also write as

$$\frac{\partial\chi^k}{\partial t} + \mathbf{u}^k\cdot\nabla\chi^k = \Gamma^k; \quad \text{with} \quad \Gamma^k \equiv (\mathbf{u}^k - \mathbf{u}_I)\cdot\nabla\chi^k, \tag{5}$$

This manipulation clearly shows that the interface velocity $\mathbf{u}_I$ reduces to $\mathbf{u}^k$ in the absence of phase change. The interface transfer flux Γ^k is such that $\sum_k \rho^k\Gamma^k = 0$, a property known as the mass jump condition.

Multiplying now the generic single-phase equations by χ and using (4) leads to the instantaneous multi-fluid equations,

$$\frac{\partial}{\partial t}(\chi^k\rho^k) + \nabla\cdot\chi^k\rho^k\mathbf{u}^k = \rho^k\Gamma^k \tag{6}$$

$$\frac{\partial}{\partial t}(\chi^k\rho^k\mathbf{u}^k) + \nabla\cdot\chi^k\rho^k\mathbf{u}^k\mathbf{u}^k = \rho^k\mathbf{u}^k\Gamma^k + \chi^k\nabla\cdot\Pi^k + \chi^k\rho^k g \tag{7}$$

where g is the acceleration of gravity, and $\Pi^k = -p^k\mathbf{I} + \sigma^{\mathbf{k}}$ is the Cauchy tensor combining pressure p and viscous stress $\sigma = \mu((\nabla\mathbf{u}) + (\nabla\mathbf{u})^{\mathbf{T}})$.

3.2. Unresolved-scale, multi-fluid flow equations

The inter-penetration of the phases and the subsequent interfacial interactions result from applying *phase averaging* to the above equations. This is the essence of the *unresolved-scale, multi-fluid* approach. The derivation of the phase average multi-fluid equations is traditionally based on the definition of the average void fraction, which could be an ensemble average, a time average, or a space average (Ishii, 1975; Drew and Lahey, 1988; Zhang and Prosperetti, 1997; Prosperetti and Zhang, 1994; Besnard and Harlow, 1988; Joseph et al., 1990). In the general case of a dependence on space and time the average void fraction may be best defined as a filtering process involving a convolution product of $\chi(\mathbf{x}', t')$ with a weighting function G (Piquet, 2013):

$$\alpha(\mathbf{x},t) \equiv \langle\chi(\mathbf{x},t)\rangle = \int G(\mathbf{x}-\mathbf{x}', t-t')\,\chi(\mathbf{x}',t')\; d^3\mathbf{x}'dt' \tag{8}$$

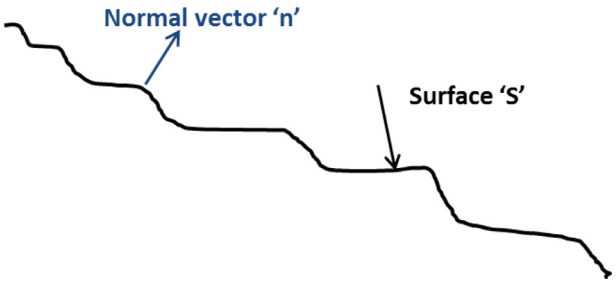

Fig. 4. Interface representation.

The weighting function characterizes the type and size of filer to be employed; the mathematical properties of which will be discussed later on. Here $\mathbf{x}'$ denotes the position of any neighboring point of $\mathbf{x}$ at time t; or, alternatively, t' denotes any instant around time t during which the quantities experience a change at point x. The choice of G is *approach-dependent* rather than *problem dependent*, in the sense that if G has to be considered within the time dimension the approach will differ from what it would be if G were taken within the spatial dimensions.

For spatially invariant properties, one can define volume averaging simply by taking G equal to zero everywhere except within integration volume V, whereas for statistically "steady" states (i.e. when the general characteristics are invariant under time translations), a time average may be useful (i.e. G is taken to equal zero outside time interval $(t - t')$). An ensemble average may also be employed,

$$\alpha(\mathbf{x},t) \equiv \langle\chi(\mathbf{x},\mathbf{t})\rangle = \lim_{N\to\infty}\frac{1}{N}\sum_{n=1}^{N}\chi^n(\mathbf{x},t) \tag{9}$$

where n represents a given sample out of a total of N samples. In all cases, $\alpha^G = 1 - \alpha^L$, and the velocity $\mathbf{u}^k$ is that of a point in the system. In the above phase average definitions, G function is explicitly taken into account as equal to unity (Slattery, 1967), but as we will see later, combining phase averaging with space filtering for LES invites to make a subtle distinction.

In the general sense, the phase-averaged equations for each phase k can now be written generically as

$$\frac{\partial}{\partial t}(\alpha^k\rho^k) + \nabla\cdot\alpha^k\rho^k\mathbf{u}^k = S_m^k \tag{10}$$

$$\frac{\partial}{\partial t}(\alpha^k\rho^k\mathbf{u}^k) + \nabla\cdot\alpha^k\rho^k\mathbf{u}^k\mathbf{u}^k = S_u^k + \nabla\cdot\alpha^k\Pi^k + \alpha^k\rho^k g - F^k \tag{11}$$

where S^k source terms are related to phase-change heat/mass transfer, while F^k denotes the averaged interfacial momentum exchange. Important to note that F^k (with $F^G = -F^L$) depends on the nature of the flow considered: for bubble-laden flows, it encompasses the drag and lift forces, the added mass, whereas for a stratified gas-liquid flow, it reflects the interfacial friction force.

3.3. Resolved-scale, single-fluid flow equations

3.3.1. Boundary conditions at a gas-fluid interface

To derive the dynamic boundary condition at a gas-fluid interface, suppose that at some instant of time the two fluids in question (k=L and k=G) are separated by a surface patch S, with the unit vector $\mathbf{n}$ pointing into the gas phase k=G (Fig. 4). The balance of forces on the surface patch S thus takes the form:

$$\int_S \mathbf{n}\cdot\mathbf{\Pi}_G\, dS + \int_S(-\mathbf{n})\cdot\mathbf{\Pi}_L\, dS + \int_S[\nabla_s\gamma - \mathbf{n}(\nabla_s\cdot\mathbf{n})\,\gamma]\, dS = 0 \tag{12}$$

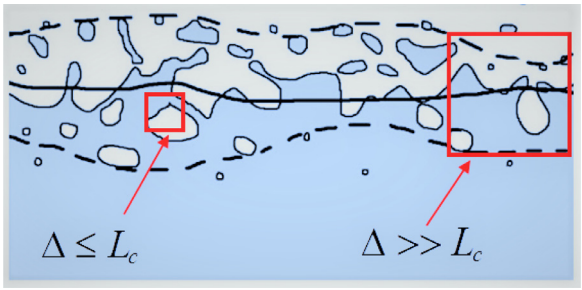

Fig. 5. SGS descriptions in the multi-fluid and single-fluid frameworks.

where we have made use of the Stokes curl theorem (to convert a contour integral to a surface integral) to derive the third term accounting for surface tension acting along the closed contour bounding the surface patch S. Note too that ∇_s is the surface gradient operator acting along the surface S, and γ is the surface tension coefficient. The first term is the force on the interface by bulk gas-phase k=G, with $\mathbf{\Pi}_G$ referring to the total stress tensor in that fluid; and the second term is the force on the interface by bulk liquid phase k=L on the other side of interface. Ordinarily, the sum of such forces must be equated to the "mass" of the surface patch multiplied by its acceleration, according to Newton's second law of motion. However, since the interface S is massless, the sum of the forces is zero not just under static conditions, but also in dynamic conditions when the surface is evolving. Combining all three terms in this expression under a single integral sign, and recognizing that the combined integral is zero regardless of the choice of the surface patch S, one obtains the differential form of the surface force balance:

$$\mathbf{n}\cdot(\mathbf{\Pi}_G-\mathbf{\Pi}_L)=\mathbf{n}\,(\nabla_s\cdot\mathbf{n})\,\gamma-\nabla_s\gamma. \tag{13}$$

If the surface tension coefficient γ is uniform along the interface, its surface gradient (which is responsible for Marangoni flows) vanishes and the stress balance takes the simplified form:

$$\mathbf{n}\cdot(\mathbf{\Pi}_G-\mathbf{\Pi}_L)=\gamma\,\kappa\,\mathbf{n} \tag{14}$$

with κ is the surface curvature evaluated at the interface defined by

$$\kappa=\nabla_s\mathbf{n}=(\nabla-\mathbf{nn}\cdot\nabla)\cdot\mathbf{n}=\nabla\,\mathbf{n}. \tag{15}$$

3.3.2. Governing equations for ITM

Reducing the length scale over which phase averaging is performed to the level where only a portion of the inclusions is present (Fig. 5) alleviates the phase inter-penetration presumed in the averaged formulation. Instead, interface jump conditions can be directly incorporated, such that the separate equations for each phase are replaced by a set of single conservation equations, with the material properties varying across the interface as this is convected with the flow. This constitutes the basis of the single-fluid formulation (Kataoka, 1986), in which the position of the front is determined by solving the topological Eq. (4), using a variety of tracking schemes; see the next subsection. Summing up the instantaneous multi-fluid mass and momentum equations (6) and (7) over phase index k yields

$$\frac{\partial\rho}{\partial t}+\nabla\cdot\rho\mathbf{u}=0 \tag{16}$$

$$\frac{\partial}{\partial t}(\rho\mathbf{u})+\nabla\cdot\rho\mathbf{uu}=\nabla\cdot\Pi+\rho\mathbf{g}+\mathbf{F}_\gamma \tag{17}$$

where the last term represents the momentum interfacial jump condition (Landau and Lifshitz, 1987) defined by

$$F_\gamma\equiv\sum_k\left[\rho^k\mathbf{u}^k\Gamma^k-\Pi^k\cdot\nabla\chi^k\right]=-(\nabla\cdot\gamma\,\mathbf{n})\;\mathbf{n}\,\delta, \tag{18}$$

This reflects the balance of the combined sum of the Cauchy stress plus the phase-change induced normal stress at the interface by surface tension. The local density ρ is defined as

$$\rho=\sum_k\rho^k\chi^k=\rho^G+(\rho^L-\rho^G)\chi, \tag{19}$$

a procedure which applies also to the local viscosity μ, although a harmonic averaging is recommended in treating viscous fluxes.

3.3.3. Commonly used ITM's schemes

Popular ITM' schemes include the Volume-of-Fluid method (VOF), the Level Set approach (LS) and the Front Tracking (FT) variant. VOF relies on the definition of the *liquid volume-fraction* occupied by one of the phases within volume V, denoted in a discrete form by F_{ijk}:

$$F_{ijk}=\frac{1}{V_{ijk}}\int_{V_{ijk}}\chi\,(\mathbf{x},t)\,dV_{ijk} \tag{20}$$

In the VOF context, the topology equation therefore, represents the evolution of the *liquid volume-fraction*, identifying flow regions containing pure liquid (where $F_{ijk}=1$) from pure gas flow regions (where $F_{ijk}=0$). Interfacial cells are such that $0<F_{ijk}<1$. The VOF method does not amount solely to the solution of

$$\frac{\partial F}{\partial t}+\mathbf{u}\cdot\nabla F=0, \tag{21}$$

it also requires accurate algorithms for advecting the volume fraction function so as to preserve conservation of mass. Since this cannot be achieved by means of conventional finite-difference schemes because of numerical diffusion, the VOF field is first advected, after which the interface location is geometrically reconstructed. The evolution of the interface is thus accomplished by reconstructing the interface within each cell and computing the volume fluxes (Scardovelli and Zaleski, 1999).

Osher and Sethian (1988) Level Set approach (LS) consists in solving the topology equation in a conventional way, while introducing a subtle mean for localizing the interface on the grid. A smooth function $\phi(\mathbf{x}, t)$ is defined everywhere in the domain, referring to the shortest distance to the front. Negative values correspond to one of the fluids and positive values to the other. The exact location of the interface corresponds to the zero level of $\phi(\mathbf{x}, t)$. When expressed in terms of the χ, the level set function is such that $\chi_k=H(\phi)$, where $H(\phi)$ is the Heaviside function defined by $H(\phi)=0$ *or* 1 if $\phi<0$ or $\phi>0$. This implies that $H(\phi)$ denotes a liquid volume fraction. The topology equation takes in this context this form:

$$\frac{\partial\phi}{\partial t}+\mathbf{u}\cdot\nabla\phi=0, \tag{22}$$

The advantage of LS is that it dispenses with interface reconstruction, it can handle merging and fragmentation, and it permits identification of the exact location of the interface. But as numerical errors cause the contours of the level set field to deform as the phase moves, a re-distancing algorithm is required to regularize the function. In other words, advecting the initial distance function $\phi(\mathbf{x}, 0)$ will not be maintained as such. An extra re-distancing algorithm preserving $|\nabla\phi|=1$ around the zero level of ϕ is required (Sussman et al., 1998). Subsequent work has focused on modifying the level set method appropriately in order to improve its mass conservation properties (Fedkiw et al., 1999).

The use of marker particles in fluid flow simulations has a long history, but the method introduced by Unverdi and Tryggvason (1992) was the first one to make it possible to simulate the time evolution of complex flows where viscosity and surface tension were important. Although new front capturing methods have now been developed that show impressive performance over earlier versions, the various variants still have difficulties to

handle with merging and breaking up of interfaces. Front tracking/capturing using markers are also known as Immersed or Embedded Boundary methods. One particularity here, is that surface tension in the momentum equation is treated as a surface force rather than as a volume force, by reference to the Continuum Surface Tension (CSF) of Brackbill et al. (1992). Other hybrid approaches combined the advantages of the methods (Enright et al., 2002) to overcome their shortcomings when applied separately; e.g. LS and VOF, or LS and particle-based FT.

4. LES Of turbulent multi-fluid flows (LEIS and LESS)

4.1. Unified filtering for multi-fluid flow

To put the derivation in context we consider a mixed multiphase flow (Fig. 5) featuring gas and liquid structures of different scales, which could be a sea surface for instance, or more precisely the foam region shown in Fig. 1. We aim at treating these flows using novel approaches transcending the conventional practice (use the two-fluid model combined with a RANS closure law) by borrowing ideas from LES, the pillar of which is the filtering process.

Filtering utilized within LES is a linear operation defined by

$$\langle f(\mathbf{x})\rangle \equiv \overline{f}(\mathbf{x}) \equiv \int_{\Omega} G(\mathbf{x}-\mathbf{x}' : \mathbf{\Delta})\, f(\mathbf{x}')\, d\mathbf{x}' \tag{23}$$

where G represents a spatial filter obeying the normalization condition:

$$\int_{\Omega} G(\mathbf{x}-\mathbf{x}' : \mathbf{\Delta})\, d\mathbf{x}' = 1 \tag{24}$$

Scales smaller than the prescribed filter width $\Delta \equiv (\mathbf{x}-\mathbf{x}')$, denoted by $f'(x) = f(x) - \overline{f}(x)$, are eliminated by the convolution product involving the kernel or weighting function $G(x-x')$, which can be Gaussian or of top-hat type. For the present, we confine the derivation to constant filter width for which commutativity of the filtering operation with respect to the differential operators is valid. For product quantities involving either χ^k or $\nabla\chi^k$, however, the commutativity principles apply with subtle modifications (Drew and Passman, 1999); one should use the Gauss rule for space derivatives,

$$\overline{\nabla\chi^k f(\mathbf{x})} \equiv \nabla\overline{\chi^k f(\mathbf{x})} - \overline{[f(\mathbf{x}) - f_I(\mathbf{x})]\nabla\chi^k} \tag{25}$$

and the Leibnitz rule for time derivatives, i.e.

$$\overline{\partial_t \chi^k f(\mathbf{x})} \equiv \partial_t \overline{\chi^k f(\mathbf{x})} + \overline{[f(\mathbf{x}) - f_I(\mathbf{x})]\mathbf{u_I}\cdot\nabla\chi^k} \tag{26}$$

The *filtered phase volumetric fraction* and its gradient are defined by

$$\overline{\chi^k}(\mathbf{x}) = \int_D G(\mathbf{x}-\mathbf{x}' : \mathbf{\Delta})\, \chi^k(\mathbf{x}')\, d\mathbf{x}' \tag{27}$$

and

$$\nabla\overline{\chi^k}(\mathbf{x}) = \int_S G^I(\mathbf{x}-\mathbf{x_I})\, \mathbf{n}\, dS \tag{28}$$

where a new filter function $G^I(\mathbf{x}-\mathbf{x_I})$ that applies on surfaces only (Sirignano, 2005) is introduced. The filter width Δ may be smaller or larger than the characteristic length scale of the dispersed phase, L_C , denoting, for example, the bubble diameter or inter-bubble spacing.

The filtered multi-fluid equations can be derived using one generic and unique filtering process which could be phrased as a *Component Weighted Volume-Averaging* (CWVA) (Lakehal et al., 2002),

$$\widetilde{f^k}(\mathbf{x}) \equiv \frac{\overline{\rho^k(\mathbf{x})\chi^k(\mathbf{x})f^k(\mathbf{x})}}{\overline{\rho^k(\mathbf{x})\chi^k(\mathbf{x})}} \tag{29}$$

In the limit of $\Delta > L_C$, were the fluids are interpenetrated (the density is thus assumed to be uniform within volume Δ^3), the above expression reduces to

$$\widetilde{f^k}(\mathbf{x})_{for\ \Delta>L_C} \equiv \frac{\overline{\chi^k(\mathbf{x})f^k(\mathbf{x})}}{\overline{\chi^k}(\mathbf{x})}, \tag{30}$$

whereas for $\Delta < L_C$, where the fluids are separated by a front (the density is thus not uniform whereas χ^k is constant at every point x^k), it should read

$$\widetilde{f^k}(\mathbf{x})_{for\ \Delta<L_C} \equiv \frac{\overline{\rho^k(\mathbf{x})f^k(\mathbf{x})}}{\overline{\rho^k}(\mathbf{x})} \tag{31}$$

4.2. The filtered multi-fluid model equations as the basis of LESS

To put the derivation in context we restrict it to the bubbly flow situations discussed previously, where the system is composed of N gas inclusions, each occupying a specific volumetric proportion. Applying first the filtering operator (23) to the system of Eqs. (6)–(7), and using (25) and (26) yields:

$$\frac{\partial}{\partial t}\overline{(\chi^k\rho^k)} + \nabla\cdot\overline{\chi^k\rho^k\mathbf{u}^k} = \overline{\rho^k\Gamma^k} \tag{32}$$

$$\frac{\partial}{\partial t}\overline{(\chi^k\rho^k\mathbf{u}^k)} + \nabla\cdot\overline{\chi^k\rho^k\mathbf{u}^k\mathbf{u}^k} = \overline{\rho^k\,\mathbf{u}^k\,\Gamma^k} + \overline{\chi^k\nabla\cdot\Pi^k} + \overline{\chi^k\rho^k}g \tag{33}$$

In order to handle with the filtered stress term, we should again resort to the Gauss rule introduced previously. Introducing now the CWVA definition (30) into the system of Eqs. 32)–((33) helps write the filtered multi-fluid equations in the form below:

$$\frac{\partial\overline{\rho}^k}{\partial t} + \nabla\cdot\overline{\rho}^k\widetilde{\mathbf{u}}^k = \overline{\rho^k\Gamma^k} + \mathcal{R}_m, \tag{34}$$

$$\frac{\partial}{\partial t}(\overline{\rho}^k\widetilde{\mathbf{u}}^k) + \nabla\cdot\overline{\rho}^k\widetilde{\mathbf{u}}^k\widetilde{\mathbf{u}}^k = \overline{\rho^k\,\mathbf{u}^k\,\Gamma^k} + \nabla\cdot\alpha^k\widetilde{\Pi}^k + \overline{\rho}^k\mathbf{g} \underbrace{-\nabla\cdot\tau^k}_{I} + \underbrace{\mathcal{R}_c}_{II} \underbrace{-\overline{\Pi_I\cdot\nabla\chi^k}}_{III} \tag{35}$$

where $\overline{\rho}^k \equiv \alpha^k\,\widetilde{\rho}^k$ and $\alpha^k \equiv \overline{\chi^k}$. The non-linearity in the convection and diffusive terms gives rise to the unresolved or SGS stress:

$$\tau^k \equiv \overline{\rho}^k(\widetilde{\mathbf{u}\mathbf{u}}^k - \widetilde{\mathbf{u}}^k\widetilde{\mathbf{u}}^k). \tag{36}$$

The mass-induced error terms $\mathcal{R}_m$ and $\mathcal{R}_c$ could be neglected in isothermal flow simulations, or when use is made of (29) instead of (30). The third unclosed quantity (III) is the filtered momentum interaction term resulting from filtering the Cauchy stress Π, including part of the interfacial forces. For dispersed bubbly flows for instance, the force exerted by the continuous phase on the bubble encompasses the drag, lift, virtual or added mass, and Basset history forces. The closure laws for these components are well documented in the literature (Auton et al., 1988).

A close inspection of the system of Eqs. (34) and (35) reveals that it is practically similar to any other time, space or ensemble averaged system, though it has a different meaning for the unclosed quantities.

4.3. The filtered mixture model equations

The filtered mixture equations follow from summing up the filtered multi-fluid mass and momentum Eqs. (34) and (35) over phases k (Lakehal and Caviezel, 2017). Assuming that the bubbles

are small and well mixed with the carrier phase, the drift/slip between the phases can be neglected and the final form of the filtered homogeneous mixture equations under isothermal conditions (no phase change is considered) read:

$$\frac{\partial \overline{\rho}^m}{\partial t} + \nabla \cdot \overline{\rho}^m \, \widetilde{\mathbf{u}}^m = 0 \tag{37}$$

$$\frac{\partial}{\partial t}(\overline{\rho}^k \alpha^k) + \nabla \cdot \overline{\rho}^k \alpha^k \, \widetilde{\mathbf{u}}^m = 0 \tag{38}$$

$$\frac{\partial}{\partial t}(\overline{\rho}^m \widetilde{\mathbf{u}}^m) + \nabla \cdot \overline{\rho}^m \, \widetilde{\mathbf{u}}^m \widetilde{\mathbf{u}}^m = \nabla \cdot (\widetilde{\Pi}^m - \tau^m) + \sum_k \overline{F^k} + \overline{\rho}^m \mathbf{g} \tag{39}$$

where we define the filtered mixture quantities as follows:

$$\widetilde{\mathbf{u}}^m = \frac{1}{\rho^m} \sum \rho^k \alpha^k \widetilde{\mathbf{u}}^k; \quad \rho^m = \sum \rho^k \alpha^k,$$
$$\Pi^m = \sum \alpha^k \Pi^k; \quad \tau^m = \sum \rho^k \alpha^k (\overline{\mathbf{u}'' \mathbf{u}''})^k; \quad u'' = u - \widetilde{u} \tag{40}$$

Note that in this simplified homogeneous formulation, all the terms involving the diffusion interphase relative velocity do not appear. Further, in case of phase change, the filtered mass conservation equation and energy equation should involve a corresponding term, which needs to be modeled as well. The interfacial term ($\sum_k \overline{F^k}$) should rigorously represent the surface tension effects on the mixture, but since the dispersed phase cannot be resolved in the phase-average context, the term should be neglected. The SGS stress tensor of the mixture τ^m can thus be defined assuming that each phasic field is a superposition of a filtered and a non-resolved part, the effect of which on momentum diffusion needs to be modeled.

4.4. The filtered single-fluid flow equations as the basis of LEIS

The filtered phase indicator function, $\overline{\chi^k}(\mathbf{x})$, in this context is interpreted as a volume-of-fluid (VOF) instead of void fraction, denoted by

$$\overline{\chi^k}(\mathbf{x}) = \int_D G(\mathbf{x} - \mathbf{x}' : \mathbf{\Delta} < \mathbf{L_C}) \, \chi^k(\mathbf{x}') \, d\mathbf{x}' \tag{41}$$

The derivation of the filtered one–fluid equations is similarly based on the use of CWVA, although performed in another form accommodating the differences in fluid flow topologies. In the filtered two–fluid formulation ((34) and (35)) the solutions generated for each phase k were weighted in interpenetrating–phase regions by the resolved volume fraction $\alpha^k(x)$, in regard to the constraint $\Delta > L_C$. However, since inter-penetration regions of the flow reduce to sharp interfaces ($\Delta < L_C$) in the single–field description, the coupling of the volume-of-fluid to the flow solution can only be represented through the local density (19). It is therefore most appropriate to use $\rho(x)$ as a basis for CWVA in this context, i.e. using (31). This is somewhat similar to the Favre averaging applied to compressible flows, but instead of using the equation of state, here the resolved density is inferred from filtering the local density,

$$\overline{\rho}(\mathbf{x}) = \overline{\chi}(\mathbf{x}) \rho^L + (1 - \overline{\chi}(\mathbf{x})) \rho^G \tag{42}$$

For mass conservation within the single–field representation, filtering of (6) using CWVA yields

$$\frac{\partial \overline{\rho}}{\partial t} + \widetilde{\mathbf{u}} \cdot \nabla \overline{\rho} = \mathcal{R}_p \tag{43}$$

where $\mathcal{R}_p$ is filtering-induced mass term. Substituting the expression of the local density into the mass conservation equation above while assuming incompressibility of the flow and no phase change leads to the filtered interface topology equations (Liovic and Lakehal, 2007; 2006; Labourasse et al., 2007):

$$\frac{\partial \overline{\chi}}{\partial t} + \widetilde{\mathbf{u}} \cdot \nabla \overline{\chi} = \mathcal{R}_\chi, \tag{44}$$

in which the local density has now been eliminated, and where $\mathcal{R}_\chi$ (which is proportional to $\mathcal{R}_p$) denotes the non-resolved interface deformations and subsequent mass transfer from one phase to the other that may have been produced by fragmentation or merging of the interface. This term has been neglected until now, but recent work devoted to the subject is likely to elucidate some of the hidden aspects.

Next, performing the convolution product (23) on the momentum Eqs. (33) and applying the CWVA filtering yields

$$\frac{\partial}{\partial t}(\overline{\rho} \, \widetilde{\mathbf{u}}) + \nabla \cdot \overline{\rho} \, \widetilde{\mathbf{u}} \, \widetilde{\mathbf{u}} = -\nabla \overline{p} + \nabla \cdot \widetilde{\sigma} + \overline{\rho} \mathbf{g} + \gamma \, \overline{\kappa} \, \overline{\mathbf{n}}$$
$$\underbrace{-\nabla \cdot \tau}_{I} + \underbrace{\mathcal{R}_d}_{II} + \underbrace{\mathcal{R}_\gamma}_{III} \tag{45}$$

where

$$\tau \equiv \overline{\rho}(\widetilde{\mathbf{u}\mathbf{u}} - \widetilde{\mathbf{u}}\widetilde{\mathbf{u}}). \tag{46}$$

The unclosed terms (II) and (III) appear in (45) as a result of non-linearity of the viscous stress and curvature κ (or the normal vector $\mathbf{n}$), i.e.

$$\mathcal{R}_d \equiv \nabla \cdot [\sigma - \widetilde{\sigma}], \tag{47}$$

$$\mathcal{R}_\gamma \equiv \gamma \, \overline{\kappa} \, \overline{\mathbf{n}} - \gamma \, \overline{\kappa} \, \overline{\mathbf{n}}. \tag{48}$$

They denote the non-resolved counterpart of interfacial drag and surface tension that have been washed out by filtering. Again, these terms which have been until now neglected are associated with potential momentum dissipation mechanisms that may be caused by unresolved interface fragmentations.

5. Unresolved or SGS turbulence

5.1. EVM as the basis SGS modeling

Both statistical and subgrid-scale modeling of turbulent multiphase flows (interpreted broadly) are far from being established. RANS or SGS models are generally based on known approaches developed in the single-phase flow context, notably centered around the linear Eddy-Viscosity Modeling (EVM) of the unclosed stresses, with some adjustments or ad-hoc measures to reflect the interaction of phases. Be it as it may, and in the absence of sufficient knowledge let us assume that for both dispersed and interfacial turbulent flows, the SGS stress tensor can still be approximated in the EVM framework:

$$\tau_{ij} = -2\mu_{sgs} \widetilde{S}_{ij} \tag{49}$$

where $\widetilde{S}_{ij}$ is the resolved strain rate. Assuming the dissipative scales to be in equilibrium, the SGS eddy viscosity μ_{sgs} may be scaled according to (Smagorinsky, 1963) using:

$$\mu_{sgs} = (C_s \overline{\Delta})^2 \rho (2 \widetilde{S}_{ij} \widetilde{S}_{ij})^{1/2} \tag{50}$$

where the model constant C_s is generally fixed ($Cs = 0.10 - 0.15$) depending on the flow. For most of LESS of dispersed-flows studies reported so far (Deen et al., 2001; Milelli et al., 2001; Capecelatro and Desjardins, 2013), the SGS stresses have been closed in the same manner, except Ničeno et al. (2008) who employed a one-equation SGS model resolving for a turbulent kinetic energy equation.

5.2. Advanced (self-adaptive) SGS modeling

The base formulation above (known as the Smagorinsky SGS model) makes SSG model grossly dissipative and ill-behaved near the wall in particular. Germano et al. (1991) derived a systematic procedure for the LES of turbulent flows without the necessity of prior experience to properly adjust the constant C_s or in better words the length scale ($C_s\overline{\Delta}$). This is known as DSM (or Dynamic Subgrid Model), and is supposedly more attractive since it implies a direct connection between the resolved and SGS flow portions, and may thus be more useful for dispersed flows where the phase interaction at the resolved-scale level is important (Lakehal et al., 2002; Yang et al., 2016). Further, in classifying the models, the DSM belongs to the so-called self-adaptive SGS models, meaning that it should virtually dispense with near-wall turbulence treatment, which stimulates its extension for interfacial flows where the gas phase perceives the interface as a moving wall boundary.

In the Variational Multiscale approach (VMS) (Hughes et al., 2001a,b), which belongs to the category of self-adaptive SGS models, too, the flow field is partitioned into coarse-scale (low wave-number) and fine-scale (high wave-number) components. The subgrid scale stress is thus made a function of the fine-scale flow field, and applies only to the fine-scale motions, meaning that energy is extracted only from high wave number modes. This is what makes the formulation outperform conventional LES models that extract energy from all modes. This was the motivation of Reboux et al. (2006) to resort to the VMS for the LEIS of a sheared interfacial flow.

5.3. Specific SGS turbulence modeling issues for bubbly flows

5.3.1. Bubble-induced diffusivity

In the multi-fluid context the presence of the dispersed phase interacting with the unresolved scale motions may contribute to the process of momentum dissipation from the resolved liquid scales (Bataille et al., 1999). This coupling effect can be interpreted as a modulation of μ^L_{sgs} in the liquid by the bubble-induced counterpart (Sato et al., 1981). By assuming the dispersed phase to follow the liquid motion at the SGS level, an SGS model was proposed by Tran (2000), in which the velocity scales of the smallest resolved motion were assumed to be comparable to the dispersed phase. The effective viscosity for the continuous phase, μ^L_{eff}, was thus augmented by an additional term reproducing the dissipation induced by SGS bubbles.

For relatively dilute bubbly-flow systems ($\alpha < 5\%$), Lakehal et al. (2002) proposed to modulate the shear-induced eddy viscosity as in Sato et al. (1981), but using now the LES ingredients:

$$\mu^L_{eff} = \mu^L_{sgs} + (C_s\overline{\Delta})\rho^L\alpha^G|\widetilde{\mathbf{u}}^L - \widetilde{\mathbf{u}}^G| \tag{51}$$

Their argument was that the bubbles may break the eddies into scales of similar size, in which case the shear- and bubble-induced dissipation mechanisms could be scaled using the same length scale ($C_s\overline{\Delta}$), in combination though with different time/velocity scales; the best-suited velocity scale of the dispersed phase would be the relative velocity $|\widetilde{\mathbf{u}}^L - \widetilde{\mathbf{u}}^G|$. Note that in the RANS framework (Sato et al., 1981; Vaidheeswaran and Hibiki, 2017), the dispersed length scale is set proportional to the bubble diameter.

5.3.2. Backscatter of energy

Further, Lakehal et al. (2002) speculated that in the LESS context it may be more meaningful to use (51) in connection with the Dynamic procedure (Germano et al., 1991) which could also deliver negative values of ($C_s\overline{\Delta}$) translating potential backscatter of energy (Mason and Thomson, 1992) from the bubbles-induced motions to the surrounding fluid flow. Indeed, use of SGS models that fix model constant C_s implies that the bubbles would systematically enhance momentum diffusivity. Recently, in analyzing the DNS data of a fully resolved bubbly channel flow (Lakehal et al., 2017), we have observed that the clustering of the bubbles near the wall has a dual effect: enhancing diffusivity near the wall where the bubbles are still of low-size, while reducing it away from the wall where the bubbles coalesce upon departure and dispersion by turbulence. Fig. 6-left compares the eddy diffusivity profiles for single-phase and bubbly-flow DNS data (same shear Reynolds number), showing clearly the bubble-induced diffusivity modulation alluded to above. The results are compared to a DNS-fitted RANS-based model introducing a modulation function $g(\alpha)$ that clearly indicates that positive and negative values of the mixing length-scale are possible, giving justice to the early speculation of Lakehal et al. (2002).

5.4. Specific SGS turbulence modeling issues for interfacial flows

5.4.1. Eddy diffusivity near sheared interfaces

For turbulent interfacial flows separated by well-defined continuous fronts, established SGS models for LES of single-phase flow could indeed be applied, but with a careful consideration of the interface layer. For instance, the SGS modeling should account for the asymptotic behavior of the turbulence quantities near the surface. Like in wall-flows, the momentum eddy diffusivity defined as

$$E_d = -\langle u'w'\rangle / \frac{d\langle u\rangle}{dz}, \tag{52}$$

should scale with the wall/interface distance as $E_d \approx z^n$, where $n = 3$ for wall flows. Many authors proposed the scaling for turbulence at free surface flows, but this should differ from sheared free-to-deform surface flows on many subtle aspects indeed. Regardless of whether the interface is wavy or flat, the eddy diffusivity has to be defined specifically for each side according to the asymptotic behavior of turbulence at the interface.

Instead of heuristically proceeding by Taylor expansion of the velocity field in the neighborhood of $z \ll 1$ inspired from wall flows (Hasegawa and Kasagi, 2007), we have recently referred to our earlier DNS data of Fulgosi et al. (2003) to establish the limiting behavior of the velocity variance components, which upon manipulation yielded first the scaling for the gas-side and liquid-side fluctuating velocities, and thus that of the shear, reading:

$$\langle u'w'\rangle = d_3 z^3 + \cdots \quad \text{Gas side}, \tag{53}$$

$$\langle u'w'\rangle = d_1 z + d_2 z^2 + \cdots \quad \text{Liquid side}. \tag{54}$$

And because the velocity gradients on both sides of the interface behaves like $d\langle u\rangle/dz = 1 + \mathcal{O}(z)$, the eddy diffusivity on the gas side behaves thus like $E_d \approx z^3$, very much the same as in wall flows, while it scales linearly with distance to the interface in the liquid side, viz. $E_d \approx z$. The proposed scaling, confirmed in the DNS data shown in Fig. 7, is understandably valid only for $z < 10$, where $d\langle u\rangle/dz \approx 1$.

Consequently, proper near-interface treatments are required to comply with the asymptotic behavior of E_d on both sides of the interface. In a similar way as in wall flows, this can be accounted for using damping functions based on distance to the interface (Reboux et al., 2006). For that purpose, analogous to the concept of a "wall units" length scale used in near-wall turbulence modeling (z^+), damping of eddy viscosity in SGS modeling close to sheared interfaces requires the introduction of its own non-dimensional length scale, denoted here by the "interface turbulence units" z^+_{Int}. Liovic and Lakehal (2007) introduced and validated the algorithm for extracting the ingredients necessary for estimating z^+_{Int} from the flow field, namely the interfacial frictional

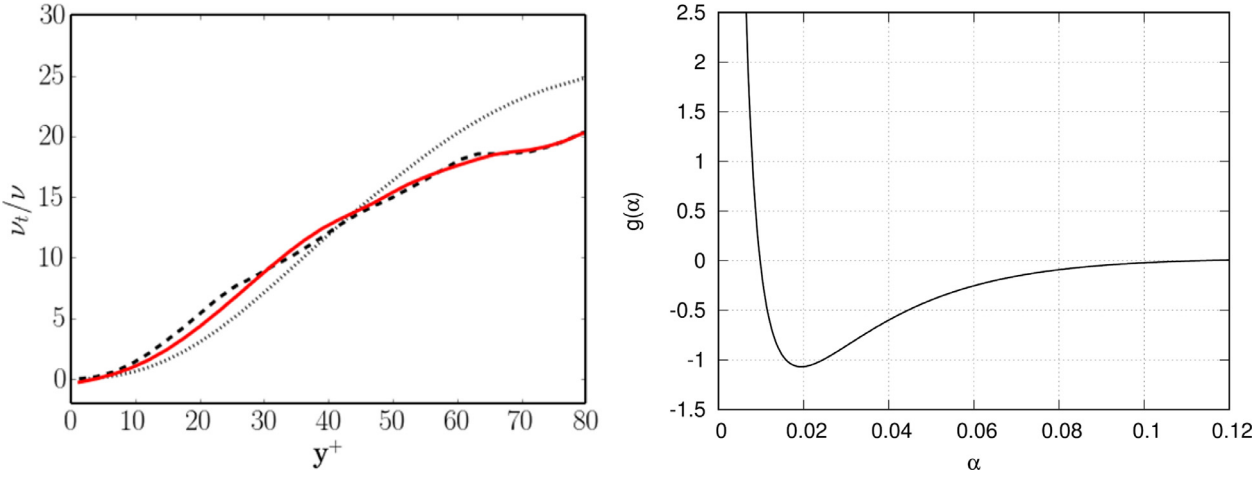

Fig. 6. (left) Normalized turbulent eddy viscosity $E_d = -\langle u'w'\rangle/(d\langle u\rangle/dz)$: DNS single-phase flow (lines); DNS bubbly flow (dotted line); DNS-based model using RANS basis ($\nu_t \equiv k^2/\epsilon$): $\nu_t^{Leff} = \nu_t^L + (g(\alpha))D\alpha^G|\bar{\mathbf{u}}^L - \bar{\mathbf{u}}^G|$ (red line). (right) DNS-fitted modulation function $g(\alpha)$. (For interpretation of the references to color in this figure legend, the reader is referred to the web version of this article.)

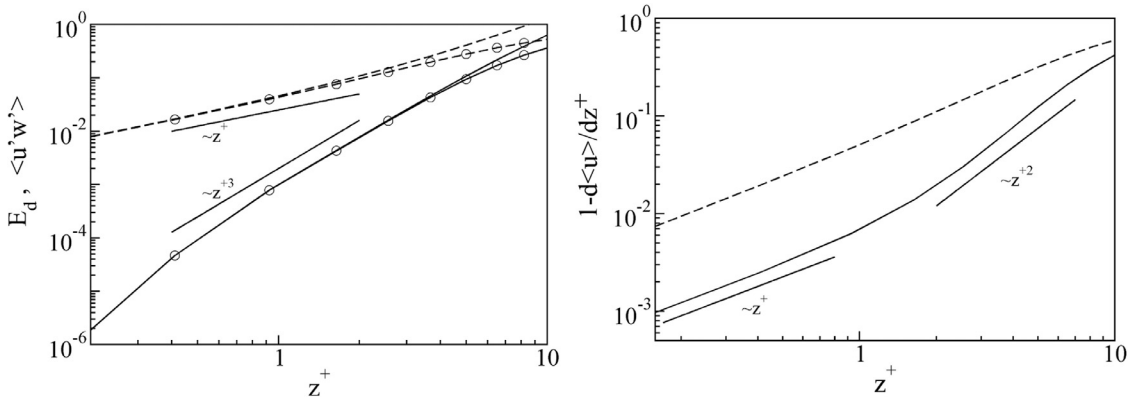

Fig. 7. DNS results of (a) turbulent eddy viscosity E_d (lines without symbols) and shear $\langle u'w'\rangle$ (lines with symbols) near the interface; (b) variations in the mean velocity gradient $1 - d\langle u\rangle/dz^+$. Plain lines: gas side; dashed lines: liquid side.

velocity $U^\tau_{\text{Int}} = (\tau_{\text{Int}}/\rho_G)^{1/2}$, and the reconstructed distance function (RDF) from raw VOF data ϕ^{RDF} defined by $z^+_{\text{Int}} = U^\tau_{\text{Int}}\phi^{\text{RDF}}/\nu^G$. Using LS is clearly advantageous in this context since the distance to the interface is directly provided by the LS function (ϕ) itself. Explicit closure of the SGS stress tensor in LEIS can be achieved within the eddy-viscosity framework discussed in the context of (49), but now with a damping function (f_μ) is introduced in order to accommodate the near-wall/interface limiting behavior discussed above; i.e. $f_{\mu\text{Int}}\,(C_s\,\overline{\Delta})^2$.

For low to moderate interface deformations, the DNS database of (Fulgosi et al., 2003) provided the following dependencies of f_μ on the distance to the interface z^+_{Int} (Fig. 8):

$$f_{\mu\text{Int}^G} = 1 - \exp\left(a\,z^+_{\text{Int}} + b\,(z^+_{\text{Int}})^2 + c\,(z^+_{\text{Int}})^3\right), \quad \text{Gas side}, \tag{55}$$

$$f_{\mu\text{Int}^L} = 1 - \exp\left(f\,z^+_{\text{Int}} + g\,(z^+_{\text{Int}})^2\right), \quad \text{Liquid side}, \tag{56}$$

where *a, b, c, f,* and *g* are model coefficients.

A systematic LES and DNS study of a counter-current sheared flow - the same as of Fulgosi et al. (2003)- performed by Reboux et al. (2006) has shown that without such modification the base model alone becomes excessively dissipative, just as it tends to be for wall-bounded flows. The comparison between full DNS (with no SGS model and a grid of $128 \times 64 \times 64$ cells), under-resolved DNS (with no SGS model and a grid of $64 \times 32 \times 32$ cells) and selected LES (with an SGS model and coarse grid) results of obtained with the reference and modified Smagorinsky models is discussed in Fig. 9 for the gas phase, where two key quantities are compared as a function of the non-dimensional distance to the interface. While the turbulent shear stress is grossly under-predicted (left panel), the fluctuations are underestimated in the streamwise directions and grossly overestimated in the other directions (right panel).The LES results (not included) in the liquid side were far off from the DNS data, probably because the eddy viscosity damping was not applied to the liquid side.

It is perhaps important to add that the experience of the author's group has shown that introducing damping at sheared interfaces can only work for stratified to stratifying flows, and is rather complex to implement for flows featuring vigorous fragmentation and coalescence, for which LEIS using VOF is better suited than with LS (Behzad et al., 2016). The DSM SGS model was found to return a sort of interface reduction of the eddy viscosity at the interface (provided it is sufficiently meshed) that could be helpful, although not rigorously obeying the strict z^3 scaling expected in the lighter phase.

5.4.2. Backscatter of energy

Reboux et al. (2006) analyzed the LES and DNS data of Fulgosi et al. (2003) to elucidate the energy transfer mechanisms returned by each SGS model for the counter-current sheared flow

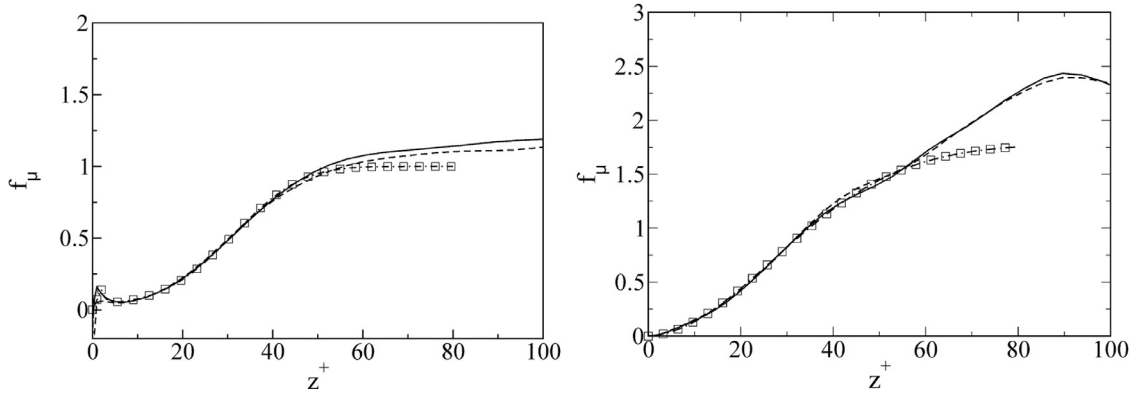

Fig. 8. DNS results of f_μ-distributions for gas (left) and liquid (right) sides for flat interface case (——) and wavy interface case (– – –) compared to the best fit to the data (□) (Fulgosi et al., 2003).

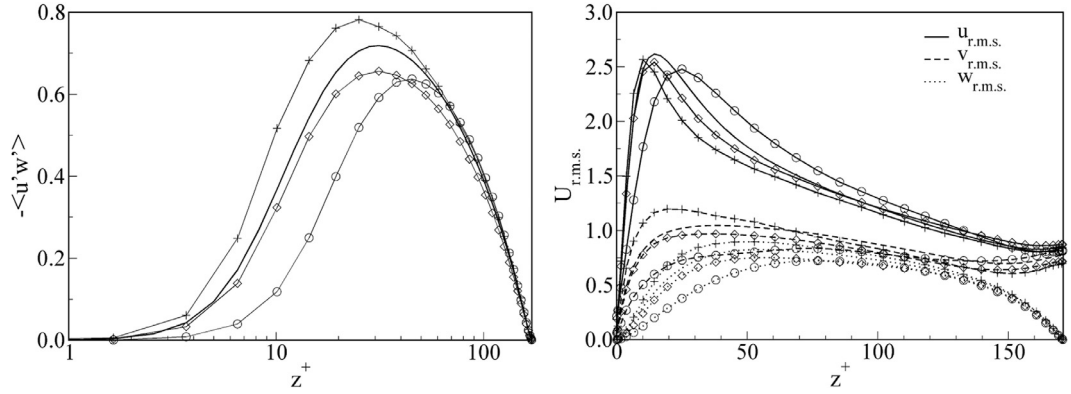

Fig. 9. Turbulence intensities and shear stress profiles in the gas phase: Lines without symbols, DNS; (+), under-resolved DNS; (○), LES with reference Smagorinsky model; (◇), LES with SGS and Eq. (55).

discussed in the earlier subsection. The comparison of the SGS models employed (LES with reference Smagorinsky model, LES with SGS and Eq. (55), and VMS) included the filtered DNS data, too. The SGS models were first applied to the filtered velocity field of the DNS, then the SGS dissipation was evaluated with the modeled stresses. The quantity of interest is what we refer to as "SGS exchange" or "SGS dissipation", governing both the top-down and bottom-up exchange of energy between the resolved and subgrid scales of turbulence:

$$\varepsilon^{SGS} = \langle \tau_{ij} \widetilde{S}_{ij} \rangle \tag{57}$$

The data were first spanwise averaged then time averaged. Positive values of the SGS dissipation indicate a flux of kinetic energy from large to small scales, and negative values indicate a bottom-up backscatter of energy.

The results are shown in Fig. 10 for both the gas and liquid sides of the interface, along with the filtered DNS data. Panels (a) and (b) of the figure show that in all cases energy is flowing from large to small scales only, meaning there is little evidence of energy backscatter. The trend is well predicted by all the SGS models employed, although the values delivered by the Smagorinsky model alone are excessively higher than the DNS. The behavior of the modified Smagorinsky model is remarkable on both side of the interface, where it compares very well to the DNS. The comparison shows an out-performance of the VMS, thanks to its capacity to control the energy transfer in the spectral domain, where energy is extracted only from high wave number modes.

In summary, the only SGS models that could potentially deal with energy backscatter (which is flow dependent) are those classified as 'self-adaptive', including DSM and VMS, augmented by near-surface treatment of turbulence.

6. Unresolved or SGS interfacial scales

6.1. SGS interphase mass transfer

Filtering is synonymous to smoothing out flow-field information that can be mass or momentum, and thus energy dissipation. An unresolved interfacial segment means a loss or gain of mass at the grid level, a quantity reflected by term $\mathcal{R}_\chi$ in (44). In other words, interface deformations can systematically be underpredicted if the interface is not well resolved or in case of grid-based filtering as employed to reduce parasitic currents induced by curvature discretization. This phenomenon is essentially independent of turbulence, albeit it can be exacerbated under strong interfacial shearing. While at the early times when LEIS has first been derived, various terms where neglected, including $\mathcal{R}_\chi$. Progress has been made since then on this particular issue; see Section 8.

6.2. SGS interphase momentum transfer

Momentum dissipation mechanisms translated in the LEIS equations by terms (I), (II) and (III) of (45) as a result of filtering cannot be simply modeled without an *a priori* order-of-magnitude analysis. Liovic and Lakehal (2007) performed such an *a priori* analysis of the unresolved surface tension in the context of 2D air bubble rise in water, on which a white-noise perturbation was superimposed to represent homogeneous isotropic tur-

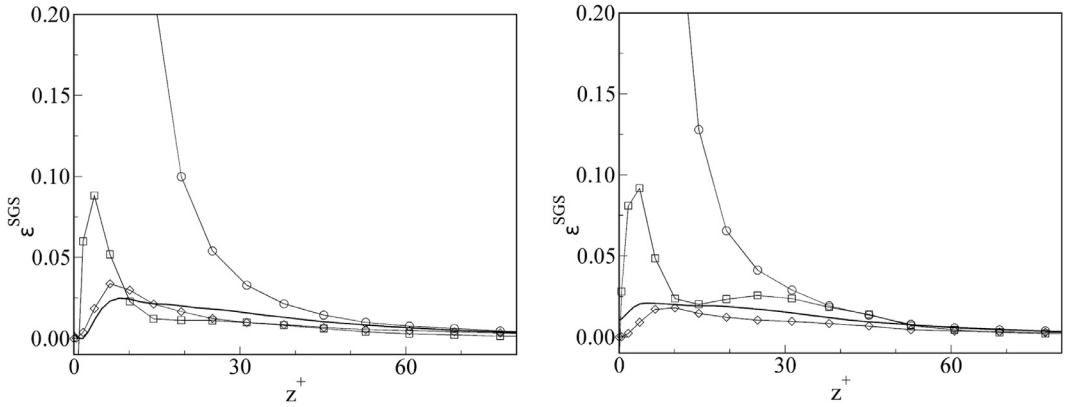

Fig. 10. SGS exchange ε^{SGS} for gas (left) and liquid (right) sides for the flat interface case. Comparison of DNS results with various SGS models: Lines, DNS; Lines with symbols, LES. (○), LES with reference Smagorinsky model; (◇), LES with SGS and Eq. (55); and (□), VMS.

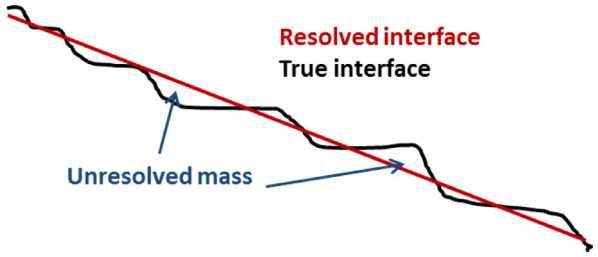

Fig. 11. Mass errors induced by unresolved interfacial scales.

bulence. Simulation re-run until a time at which smaller-scale interface wrinkling became noticeable, then beyond, until more substantial turbulence-induced interface wrinkling appeared (Fig. 11). Filtering of the data using a tophat filter was then performed to generate the SGS terms for comparison: $\nabla \cdot \tau|_i$ and $\epsilon_\gamma|_i$.

Comparing the ratio of these two SGS terms revealed that, for the most part, unresolved surface tension in the interface support is two orders of magnitude smaller than the SGS turbulence stress term (Fig. 12). The areas showing the unresolved surface tension to locally be larger than the SGS stress were visible on the fringes of the interface support, where the smeared-interface CSF computation of the interface normal estimation is not overlapped by the more interface-localized SGS stress distribution. The study asserted that unresolved surface tension can be categorized as "small" for flow problems with relatively well-resolved interfaces, but is not necessary true for fragmentation-dominated flows, like jet atomization for instance. A similar analysis was being performed in parallel (Vincent et al., 2008; Toutant et al., 2009).

The second term, $\mathcal{R}_d$, resulting from filtering the viscous stress has traditionally been neglected – without rigorous arguments – in variable-density compressible flows. In fact, this term reflects the unresolved drag force related to the SGS structures. No *a priori* order-of-magnitude analysis is to be reported; probably because, in contrast to Term III, a full 3D DNS is required for the purpose, e.g. jet atomization.

6.3. SGS curvature modeling

Using the CSF formulation of Brackbill et al. (1992) in the LEIS context implies that the surface tension consists of resolved-scale and SGS contributions to curvature and surface normal-vector: $\overline{\kappa}$ and κ^{SGS}, and $\overline{\hat{n}_i}$ and $\hat{n}_i^{SGS}$. But the difficulty of the subject is that in all interface resolving approaches, surface tension is always artificially filtered to control parasitic currents, independently from the grid and from the flow (laminar or turbulent).

Alajbegovic (2001) proposed a general form for an SGS curvature model that is linked to the SGS turbulence scales: $\kappa(\mathbf{x}) = \overline{\kappa(\mathbf{x})} + \kappa'(\mathbf{x})$. The unresolved curvature is made proportional to the resolved part via a closure coefficient C, which, he claims, must be a functional of resolved SGS stresses, i.e. $\kappa'(\mathbf{x}) = \Delta C \overline{\kappa(\mathbf{x})}$. The justification by Alajbegovic (2001) for the linkage of SGS surface tension and stresses is also not obvious, given the curvature (resolved or SGS) is specifically a property of interface topology: unresolved surface tension can also manifest itself in laminar interfacial flows.

Herrmann and Gorokhovski (2008) and later on Herrmann (2013) proposed explicit filtering based on knowledge of "exact" curvatures and normals, and relying on a refined level-set method to represent the exact interface. While potentially useful for some subset of multi-material flow scenarios, the use of refinement-based techniques limits its widespread applicability.

Liovic and Lakehal (2012) proposed an alternative approach to modeling unresolved curvature based on additional *coarse-grid* representations of the interface, a true SGS reconstruction or deconvolution approach to quantifying unresolved surface tension. In other words, based on the analogy with conventional LES of turbulent flows, in this model the resolved distributions are used to compute the resolved surface force $\gamma \overline{\kappa}\ \overline{n_i}\delta$, and then the unresolved surface force terms (κ^{SGS} and $\hat{n}^{SGS}$) is modeled based on a procedure for interrogating interface geometry.

Recently, Aniszewski et al. (2012) have shown using a priori DNS simulations that the negligibility assumption of the unresolved surface tension can be challenged. They proposed a model for one of the sub-grid two-phase specific terms, using deconvolution of the velocity field and advection of the interface using that field. Numerical tests could be presented assessing the model's performance by comparison with a priori DNS results.

7. Extension to phase-change heat transfer problems

If the majority of multi-phase flow problems are in reality turbulent and inherently unsteady, a non-negligible part of these features in addition mass transfer or phase-change induced by heat transfer under one form or another: boiling, evaporation and condensation.

The LEIS concept has been recently updated to cope with condensing heat-transfer problems under turbulent flow conditions by Lakehal and Labois (2011). The basic modeling framework is the same as described above, a part from the fact that the topology Eq. (19) should now involve the interphase mass-transfer source term

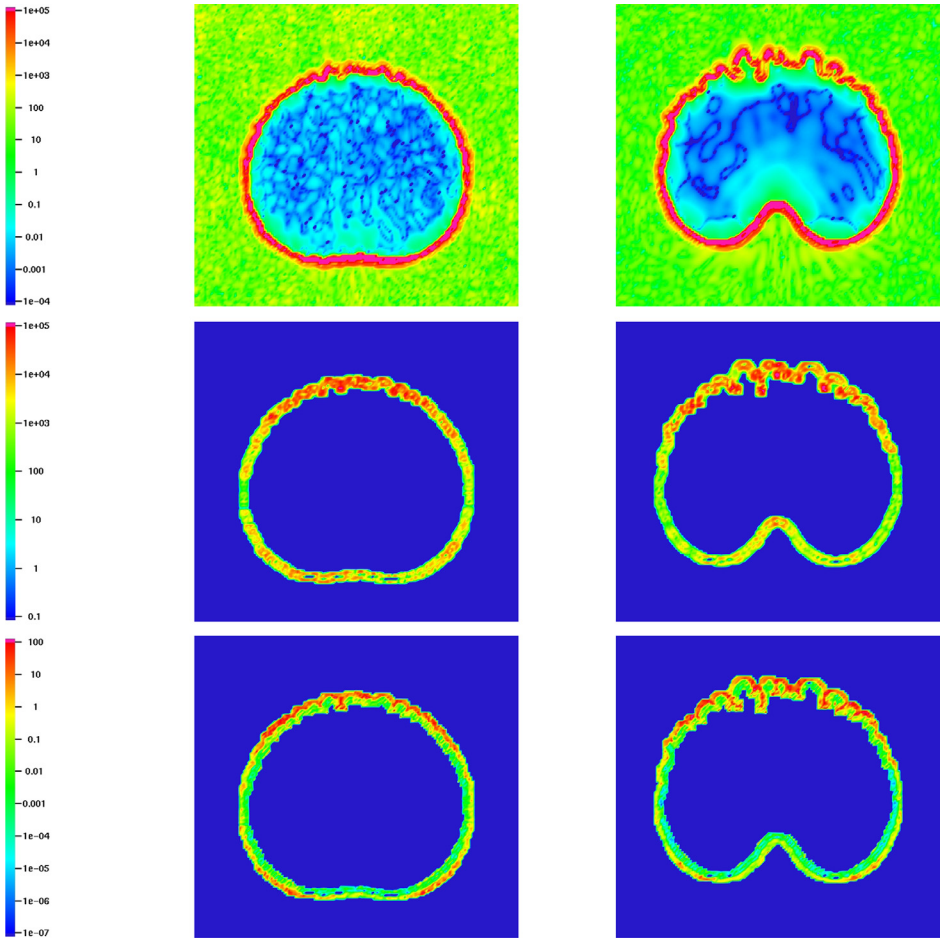

Fig. 12. Distributions at two time steps T2 and T3 resulting from a priori evaluation applied to DNS results of 2D bubble rise: row 1 quantities the SGS stress term I ($|\partial\tau_{xy}/\partial x + \partial\tau_{yy}/\partial y|$), row 2 shows the unresolved surface tension term IV ($|\epsilon_{2_Y}|$), and row 3 shows their ratio.

Γ^k, translated into a phase change velocity defined by $K = \dot{m}/\rho$ [m/s], with $\dot{m}$ standing for the rate of interfacial mass transfer $[kg/m^2.s]$.

In case the interfacial sublayer is grid-resolvable, the rate of mass transfer is determined using the energy jump condition $\dot{m}h_{SL} = (q''_S - q''_L)$, where h_{SL} is the latent heat of phase change and $q''_k = -(\lambda_k \nabla T_k)$ are the steam and liquid heat fluxes that should be directly integrated on the underlying grid, instead of resorting to 'wall-layer' like models. By analogy with turbulent flows, this could be interpreted as a low-Re wall-resolving approach, which is understandably expensive for practical 3D problems. But since in most of practical high-Re flow and high sub-cooling rate problems the interfacial sublayer cannot be resolved, use should be made of interphase mass transfer models (in the liquid side which acts as a buffer layer resisting phase change), formulated in terms of Nusselt number (Nu_L) or heat transfer coefficient (HTC) . Use of option (i) or (ii) depends on the nature of the problem under consideration: component-scale problems can only be treated with option (ii) indeed, while option (i) remains applicable to microscale problems.

Be it as it may, option (ii) is described in detail by Lakehal and Labois (2011). Briefly, interfacial heat transfer correlations are essentially based on the eddy model concept (Banerjee and MacIntyre, 2004), in which the normalized transfer velocity by the interfacial shear-velocity ($K^+ = K/U^\tau_{\text{Int}}$) is expressed in terms of dimensionless numbers that are relevant to the fluid and flow and heat transfer, i.e. the turbulent Reynolds number and Prandtl number: $K^+ \equiv Re_t^m\, Pr_L^n$, where exponents m and n are model coefficients. Several other forms of parameterization were suggested, including the so-called Surface Divergence Theory (Banerjee et al., 2004; Lakehal et al., 2008), and its Scale-adaptive variant (Lakehal and Labois, 2011); the latter has proven to work best for a range of turbulent condensing flow problems.

While the LESS approach has also been extended to tackle condensing interfacial flows using mass-transfer models evoked above, the approach is clearly ill-posed since the interfacial shear-velocity U^τ_{Int} on which most of the models are based - is less well defined due to diffusion-induced smearing. To avoid this constraint, various published contributions propose ad-hoc interface sharpening schemes.

Clearly, if the superiority of LEIS over LESS is established for condensing interfacial flows, the contrary is true of phase-change dispersed flows. One of which being wall-boiling flows which physically involve nucleate boiling preceding departure from the wall and migration under the action of the wall heat flux. LEIS is not applicable for bubbly flows anyway; use of LEIS to predict a turbulent convective flow boiling along a fuel rod and in a turbulent channel flows has indeed been attempted by Caviezel et al. (2013) and Metrailler et al. (2015), who proposed a SGS wall-boiling model to avoid having to artificially initiate steam bubbles on the wall. The mesh requirement was such that a dry out film on the wall was obtained rather than a steam layer.

In a very recent contribution by the group (Lakehal and Caviezel, 2017) though, LESS under the homogeneous form of it (37) has been applied to predict the same convective flow boil-

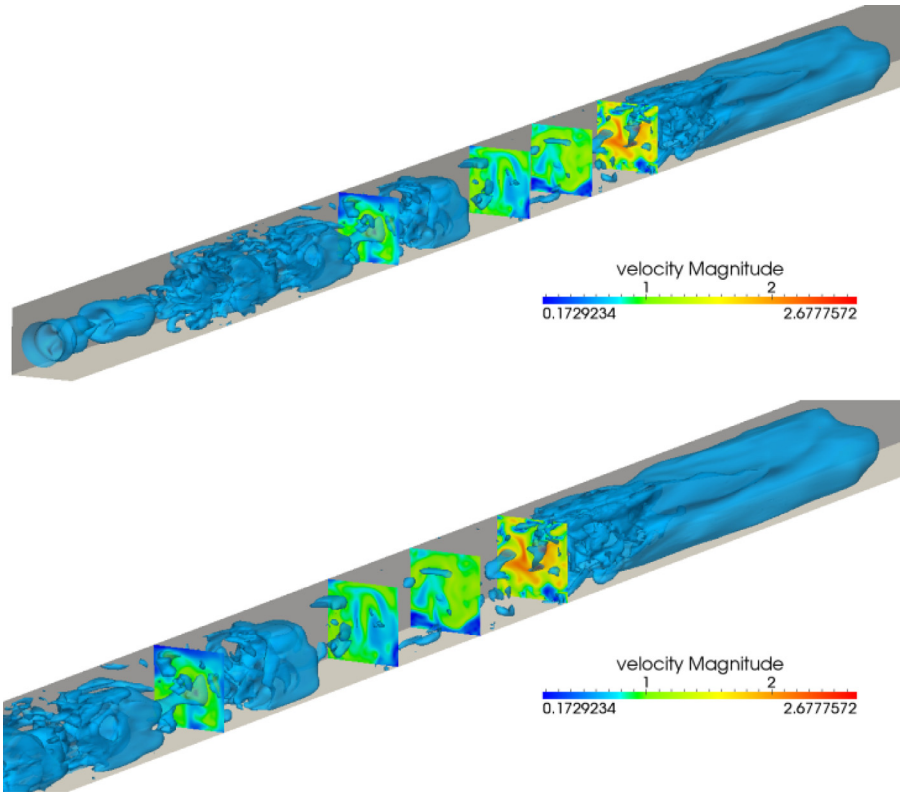

Fig. 13. LEIS of slug flow in a vertical closed channel.

ing along a fuel rod at a medium Reynolds number and medium sub-cooling rate. In order to trigger steam bubbles on the rod a wall-boiling model has been incorporated (e.g. the so-called triple-flux partition model), in which the rate of generated steam at wall locations approaching saturation temperature is determined through evaporation and 'speculated' quenching processes, mimicked by deterministic models; typically the same sort of models employed in 1D system codes. Concerning turbulence though, the study has revealed that the quality of the results does not necessarily depend on the SGS model employed for turbulence.

8. Peripheral and required developments

8.1. Multiscale issues: the ARM model

If multi-fluid flows are in general turbulent, a majority of these do feature multiscale issues, where large interfaces (stratified, slug and annular flows) co-exist with dispersed (bubbly flows) and mixed (churn flow) systems. This is well illustrated in Fig. 13 below depicting LEIS results of a slug flow in a vertical closed channel. Evidence from various lab-experiments suggests that the wake of the ascending slug is generally populated with individual gas bubbles, which the LEIS alone would not capture because of insufficient grid resolution. The same issue can be identified in the spilling wave sketched in Fig. 1 and in atomizing liquid jets. To cope with such multiscale issues, there is a need to couple LEIS with LESS under one unified predictive strategy. This is the spirit of the ARM model, short for All-Regime Multi-fluid model, the idea of which is to predict large resolved interfaces together with subscale dispersed entities that may be generated from the sheared interface itself.

ARM is based on segregating the flow system into two fields (Fig. 14) separated by a large grid-resolved interface, each being

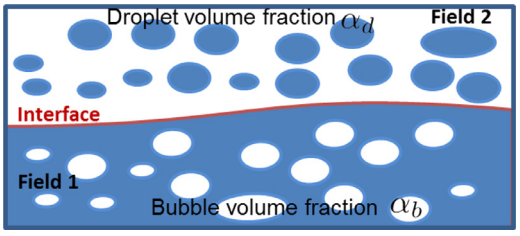

Fig. 14. Field and interface representation in ARM.

populated by dispersed phases, gas bubbles (α_b) or liquid droplets (α_d). The liquid field is marked by $H = 1$, whereas the gas field by $H = 0$ (use is made of H to differentiate with ITM, where the gas and liquid phases are marked by $\chi = 0$ and 1). Thus, the volume fraction of subscale bubbles in the liquid phase is $H\alpha_b$, while the volume fraction of gas in the gaseous phase is $(1-H)(1-\alpha_d)$. Similarly, $H(1-\alpha_b)$ is the volume fraction of subgrid droplets in the liquid phase. The total volume fractions of gas and liquid can be defined as:

$$\alpha^G = H\ \alpha_b + (1-H)(1-\alpha_d) \tag{58}$$

$$\alpha^L = H(1-\alpha_b) + (1-H)\alpha_d \tag{59}$$

It can easily be shown that the amount of bubbles α^G and droplets α^L is within the range [0, 1]. The density is defined as $\rho = \rho_G\alpha^G + \rho_L\alpha^L$. Next we make the assumption that the flow is homogeneous, implying $u^G_{g,j} = u^G_{l,j} = u^G_j$ and $u^L_{g,j} = u^L_{l,j} = u^L_j$. From the principle of mass conservation, together with the assumptions of absence of phase change and divergence free velocity u_j, the system of phasic mass & topology equations for the dispersed phases

(bubbles, and droplets) and the interfacial field can be written as:

$$\frac{\partial \alpha_b}{\partial t} + u_j \frac{\partial \alpha_b}{\partial x_j} = \Gamma^b, \tag{60}$$

$$\frac{\partial \alpha_d}{\partial t} + u_j \frac{\partial \alpha_d}{\partial x_j} = \Gamma^d, \tag{61}$$

$$\frac{\partial H}{\partial t} + u_j \frac{\partial H}{\partial x_j} = \Gamma^H. \tag{62}$$

where the transfer rates Γ^b , Γ^d and Γ^H (= $\mathbf{u}^H \nabla H$, with $\mathbf{u}^H$ being the interface velocity) are connected through the constraint

$$(1 - \alpha_b - \alpha_d)\ \Gamma^H = 0. \tag{63}$$

Note in particular that the third equation of the above system has the exact form of Eq. (5). This leaves two degrees of freedom to model the transfer rates Γ^b and which should be modeled using local resolved variables, whereas the interface transfer flux Γ^H must obey the interface constraint (63). Positive or negative values of Γ^b reflects the mass transfer of gas in and out of Field 1, and the same is true for Γ^d , which should translate the mass transfer of liquid in and out of Field 2. While a positive value of Γ^H implies now an interphase transfer from the interface to Field 1 (e.g. interface pinching or tearing-off into droplets), a negative value means a transfer to Field 2, always from the interface. The present formulation of ARM was purposely simplified to validate the principle, a more complete variant including drift velocities between each field has been derived and is now under testing. These three terms may be additionally augmented by other contributions accounting for phase-change heat transfer.

The combined fields are treated by a global mixture momentum equation that accounts though (in contrast to base mixture model presented earlier) for the separation of the two fields by means of surface tension (F_γ) :

$$\frac{\partial}{\partial t}(\rho^m \mathbf{u}^m) + \nabla \cdot \rho^m \mathbf{u}^m \mathbf{u}^m = \nabla \cdot \Pi^m + \nabla \cdot \alpha^k(\sigma^k) + F_\gamma + \rho^m g \tag{64}$$

8.2. Unresolved interphase mass transfer

Unresolved mass transfer (interpreted by the transfer rate Γ^H in Eq. (62)) modeling was conducted via an a-priori analysis of refined simulation data. The objective is to estimate the rate of mass transfer dissipated (unresolved) by use of ITM applied on non-sufficiently fine grids, be it under laminar or turbulent flow conditions. We use for the purpose the data from a selected flow exhibiting strong surface fragmentation into bubbles, namely the jet-plume experiment of Castillejos (1986), in which air is injected at the bottom of a cylindrical water tank from a 6 mm diameter nozzle at a mass flow rate of 880 cm^3/s. The experiment presents a range of bubble sizes ranging from 1 mm to 6 cm, which makes it difficult to model with phase-average models because of the difficulty to set up correlation for the closure laws when the range of bubble size and shapes is so wide. A full resolution of every interfacial scale would understandably be prohibitive.

The experiment was first simulated with the LESS approach described above under the mixture formulation with an Algebraic Slip Model (ASM) for the drift, then with LEIS based on the Level-Set for surface tracking, using a medium grid consisting in 700.000 cells. Subgrid-scale turbulence modeling was achieved using the Dynamic model (Germano et al., 1991) in both simulations.

The comparison shown in Fig. 15 between the two sets of results revealed that the flow can indeed be predicted with equal details near the injection, but differences appear immediately downstream: while LEIS tends to filter out the smaller structures, LESS tends rather to smear all the scales into a bubbly cloud. The second step consists in solving on a finer grid (2 million cells) the flow using LEIS only, where a larger portion of the interfacial scales is now resolved. This detailed simulation revealed another picture as depicted in Fig. 16, featuring large and small-scale structures that could not be tracked on the medium grid.

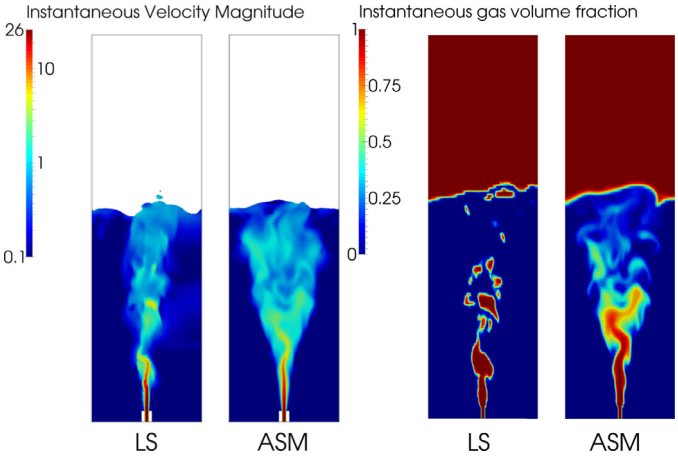

Fig. 15. LEIS (using Level Set) and LESS (using mixture ASM) of Castillejos' bubbly plume flow: medium grid resolution.

We then proceeded by analyzing the flow in detail, looking at all local resolved quantities that could be of relevance to modeling. This was achieved by filtering the fine-grid flow field and performing an a-priori analysis of the data. Intuitively, the ingredients needed for SGS mass transfer modeling should include resolved flow-field information, including the rate of strain and vorticity tensors, but also filtering parameters, and surface force details translated by the Weber number. A combination of these flow quantities and fluid parameters using the Pi-Theorem ($\mathbf{u}^H_{model} = f(We, Re_\tau, \widetilde{H}(x), \widetilde{S}_{ij})$ and systematic comparison with the fine-grid data and their filtered counterparts led to a model for interface velocity $\mathbf{u}^H$ (and thus the transfer rate Γ^H) denoting its fragmentation due to the unbalance between friction and surface tension:

$$\mathbf{u}^H_{model} = (We^{-1/2}\overline{\Delta})^2 \rho \sqrt{2\widetilde{S}_{ij}\widetilde{S}_{ij}}\ \partial \widetilde{H}/\partial x_j \tag{65}$$

The above subgrid-scale model is in fact pretty much similar to the conventional EVM closure laws for scalar fluxes, including for the flame propagation G-equation (Im et al., 1997), although it is not necessarily linked to the SGS eddy viscosity and should be applicable to all flow regimes. The key difference with the other EVM models applied for scalar fluxes is that the model constant here is dictated by physics. The model was found to compare very well with the LEIS data, as shown in Fig. 17 depicting the iso-contours of the ratio of the modeled ($\mathbf{u}^H_{model}$) to the filtered interface velocity values ($\mathbf{u}^H_{filtered}$) at one time instant. The figure clearly shows that the models predicts an unresolved mass-transfer term always located inside the gas phase, with higher magnitude inside large structures which tend to fragment (the ratio tending towards unity) and smaller values in small bubbles. The lower panel in the figure presents the distribution of $\mathbf{u}^H_{model}$ in the domain, showing that it returns higher values at the interface seen from the gas-phase side, where potential fragmentation of the interface into small bubbles is expected. Further validation of the model is underway.

In summary, the model can be applied in connection with LEIS only in the context of a hybrid approach similar to ARM, capable to treat resolved large interfaces and unresolved dispersed phases.

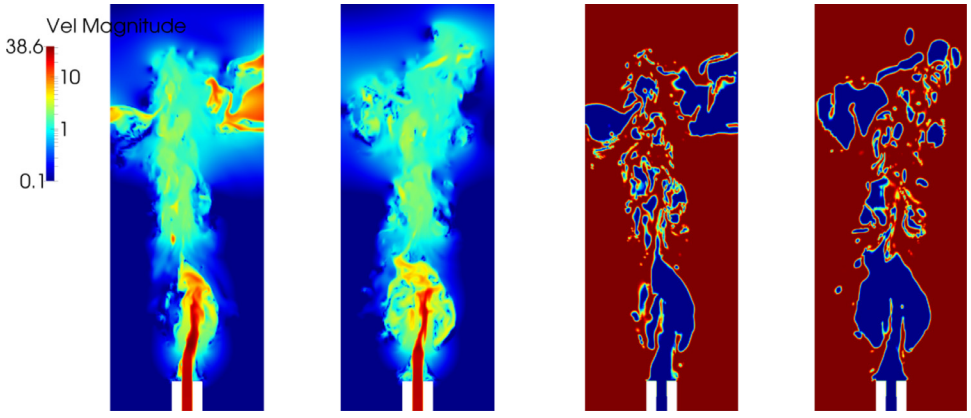

Fig. 16. Fine grid LEIS of Castillejos' bubbly plume flow. (left) velocity contours; (right) resolved interface.

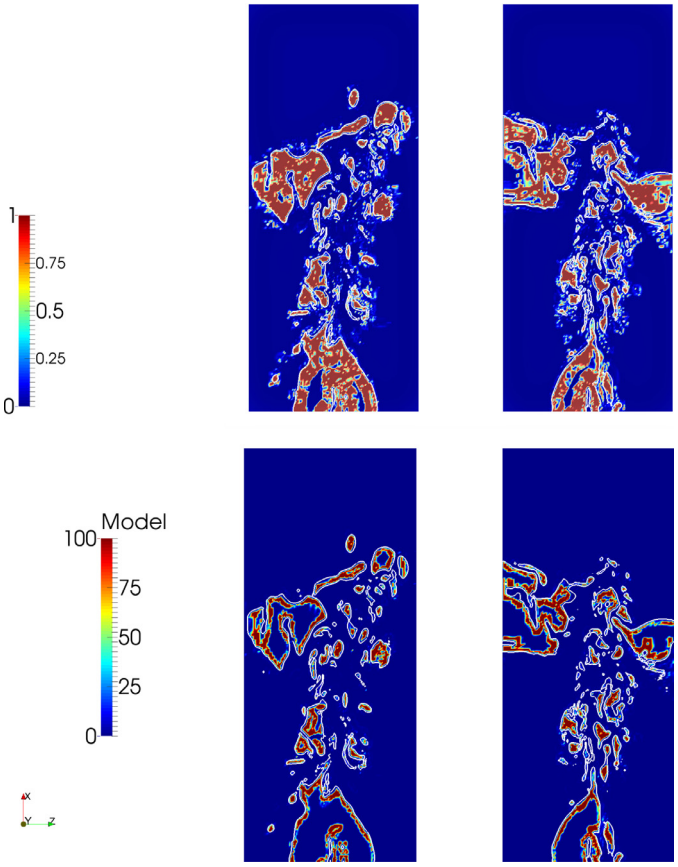

Fig. 17. (upper panel) Iso-contours of the ratio ($\mathbf{u}^H_{model}/\mathbf{u}^H_{filtered}$); (lower panel) Iso-contours of $\mathbf{u}^H_{model}$ calculated using (63).

9. Conclusions

The paper describes the way computational multi-fluid flow scene is migrating to more sophisticated modeling techniques, transcending the combination of phase-average and statistical time-average formulations by extending the base predictive strategies to the LES framework, leading to the concepts of LEIS and LESS. The methods can be successfully applied to generate realistic transient simulations of turbulent interfacial and dispersed flows using reasonable computing resources. The perspectives for extension and generalization of such strategies to a variety of practical problems are real, in view of the ever-increasing computational resources. However, we are still far from the computational power needed to fully simulate very complex situations that involve multiscale issues. The paper provides enough derivation details about each model as well as the connection between the supergrid and subgrid physics. The paper also proposes further new developments for more complex multiscale, multi-fluid flow problems.

References

Alajbegovic, A., 2001. Large eddy simulation formalism applied to multiphase flows. In: Proceedings of ASME Fluids Engineering Division Summer Meeting New Orleans, FEDSM2001-18192.
Aniszewski, W., Bogusawski, A., Marek, M., Tyliszczak, A., 2012. A new approach to sub-grid surface tension for LES of two-phase flows. J. Comput. Phys. 231 (21), 7368–7397.
Auton, T., Hunt, J., Prud'homme, M., 1988. The force exterted on a body in inviscid unsteady non-uniform rotational flow. J. Fluid Mech. 197, 241–257.
Banerjee, S., Lakehal, D., Fulgosi, M., 2004. Surface divergence models between turbulent streams. J. Multiph. Flow 30/7-8, 965–979.
Banerjee, S., MacIntyre, S., 2004. The air-water interface: turbulence and scalar exchange. Ind. Eng. Chem. Fundam. 7, 22.
Bataille, J., 1981. Averaged Field Equations for Multiphase Flows. Brown University.
Bataille, J., Marie, J., Lance, M., 1999. Turbulence in bubbly blow: from experiments to numerical modelling. In: Proceedings of the 2nd International Symposium on Two-Phase Flow Modelling and Experimentation. Piza, Italy.
Behzad, M., Ashgriz, N., Karneya, B., 2016. Surface breakup of a non-turbulent liquid jet injected into a high pressure gaseous crossflow. Int. J. Multiph. Flow 80, 100–117.
Besnard, D., Harlow, F., 1988. Turbulence in multiphase flow. Int. J. Multiph. Flow 14 (6), 679–699.
Brackbill, J., Kothe, D., Zemach, C., 1992. A continuum method for modeling surface tension. J. Comput. Phys. 100, 335–354.
Buonfiglioli, M., Mendonça, F., 2005. LES-VOF Simulation of Primary Diesel Spray Break-up with Synthetic Inlet Perturbations. ILASS Americas.
Capecelatro, J., Desjardins, O., 2013. An euler-lagrange strategy for simulating particle-laden flows. J. Comput. Phys. 238, 1–31.
Castillejos, A.H., 1986. A Study of the Fluid-Dynamic Characteristics of Turbulent Gas-Liquid Bubble Plumes. Ph.D. thesis. University of British Columbia.
Caviezel, D., Narayanan, C., Lakehal, D., 2013. Large eddy & interface simulation (leis) of turbulent flow and convective boiling in a pwr rod bundle. In: Proceedings of the 8th International Conference on Multiphase Flow (ICMF). Korea.
Chesnel, J., Reveillon, J., Menard, T., Demoulin, F.-X., 2011. Large eddy simulation of liquid jet atomization. Atomization Sprays 21 (9), 711–736.
Crocco, L., Cheng, S.-I., 1956. Theory of Combustion Instability in Liquid Propellant Rocket Motors. Technical Report. Princeton University NJ.
Deen, N.G., Solberg, T., Hjertager, B.H., 2001. Large eddy simulation of the gas–liquid flow in a square cross-sectioned bubble column. Chem. Eng. Sci. 56 (21), 6341–6349.
Desjardins, O., Pitsch, H., et al., 2010. Detailed numerical investigation of turbulent atomization of liquid jets. Atomization Sprays 20 (4), 311.
Drew, D., Lahey, R., 1988. The three-dimensional time and volume averaged conservation equations of two-phase flow. Adv. Nucl. Sci. Technol. 20, 1–69.
Drew, D., Passman, S., 1999. Theory of Multicomponent Fluids. Springer, New York, USA.
Duret, B., Reveillon, J., Menard, T., Demoulin, F., 2013. Improving primary atomization modeling through DNS of two-phase flows. Int. J. Multiph. Flow 55, 130–137.

Elghobashi, S., Truesdell, G.C., 1993. On the two–way interaction between homogeneous turbulence and dispersed solid particles. I. Turbulence modification. Phys. Fluids A: Fluid Dyn. 5, 1790–1801.

Enright, D., Fedkiw, R., Ferziger, J., Mitchell, I., 2002. A hybrid particle level set method for improving interface capturing. Comput. Phys. 183, 83–116.

Fedkiw, R., Aslam, T., Merriman, B., Osher, S., 1999. A non-oscillatory eulerian approach to interfaces in multimaterials flows (the ghost fluid method). J. Comput. Phys. 152, 457–492.

Ferrante, A., Elghobashi, S., 2003. On the physical mechanisms of two-way coupling in particle-laden isotropic turbulence. Phys. Fluids 15, 315–329.

Fox, R.O., 2012. Large-eddy-simulation tools for multiphase flows. Annu. Rev. Fluid Mech. 44, 47–76.

Fulgosi, M., Lakehal, D., Banerjee, S., DeAngelis, V., 2003. Direct numerical simulation of turbulence in a sheared air–water flow with deformable interface. J. Fluid Mech. 482, 310.

Germano, M., Piomelli, U., Moin, P., Cabot, W., 1991. A dynamic subgrid-scale eddy viscosity model. Phys. Fluids 3, 1760–1765.

Hasegawa, Y., Kasagi, N., 2007. Effects of interfacial velocity boundary condition on turbulent mass transfer at high schmidt numbers. Int. J. Heat Fluid Flow 28 (6), 1192–1203.

Hélie, J., Khan, M.M., Gorokhovski, M., 2016. Large eddy simulation of a turbulent spray jet generated by high-pressure injection: impact of the in-nozzle flow. J. Turbul. 17 (9), 823–846.

Herrmann, M., 2013. A sub-grid surface dynamics model for sub-filter surface tension induced interface dynamics. Comput. Fluids 87, 92–101.

Herrmann, M., Gorokhovski, M., 2008. An outline of an LES subgrid model for liquid/gas phase interface dynamics. In: Proceedings of Summer Program – Center for Turbulence Research Stanford.

Hirt, C.W., Nichols, B.D., 1981. Volume of fluid (VOF) method for the dynamics of free boundaries. J. Comp. Phys. 39, 201.

Hughes, T., Mazzei, L., Oberai, A., Wray, A., 2001. The multiscale formulation of large-eddy simulation: decay of homogeneous isotropic turbulence. Phys. Fluids 13(2), 505–512.

Hughes, T., Oberai, A., Mazzei, L., 2001. LES of turbulent channel flows by the variational multiscale method. Phys. Fluids 13/6, 1784–1799.

Im, H.G., Lund, T.S., Ferziger, J.H., 1997. Large eddy simulation of turbulent front propagation with dynamic subgrid models. Phys. Fluids 9 (12), 3826–3833.

Ishii, M., 1975. Thermo-Fluid Dynamic Theory of Two-Phase Flow. Eyrolles, Paris, France.

Jarrahbashi, D., Sirignano, W., 2014. Vorticity dynamics for transient high-pressure liquid injection a. Phys. Fluids 26 (10), 73.

Joseph, D., Lundgren, T., R., R.J., Saville, D., 1990. Ensemble averaged and mixture theory equations for incompressible fluid-particle suspensions. Int. J. Multiph. Flow 16 (1), 35–42.

Kaario, O., Vuorinen, V., Hulkkonen, T., Keskinen, K., Nuutinen, M., Larmi, M., Tanner, F.X., 2013. Large eddy simulation of high gas density effects in fuel sprays. Atomization Sprays 23 (4).

Kataoka, I., 1986. Local instant formulation of two-phase flow. Int. J. Multiph. Flow 12, 745–758.

Klein, M., Kasten, C., Gao, Y., Chakraborty, N., 2015. A-Priori direct numerical simulation assessment of sub-grid scale stress tensor closures for turbulent premixed combustion. Comput. Fluids 122, 1–11.

Labois, M., Lakehal, D., 2011. Very-large eddy simulation (v-les) of the flow across a tube bundle. Nucl. Eng. Des. 241 (6), 2075–2085.

Labourasse, E., Lacanette, D., Toutant, A., Lubin, P., Vincent, S., Lebaigue, O., Caltagirone, J.-P., Sagaut, P., 2007. Towards large eddy simulation of isothermal two-phase flows: governing equations and *a priori* tests. Int. J. Multiph. Flow 33, 1–39.

Lakehal, D., 2004. DNS and LES of turbulent multifluid flows. In: Proceedings of the 3rd Symposium of Two-Phase Flow Modelling and Experimentation. Pisa.

Lakehal, D., 2010. Leis for the prediction of turbulent multifluid flows applied to thermal-hydraulics applications. Nuclear Eng. Des. 240, 2096–2106.

Lakehal, D., Caviezel, D., 2017. Large-eddy simulation of convective wall-boiling flow along an idealized PWR rod bundle. Nucl. Eng. Des. 321, 104–117.

Lakehal, D., Fulgosi, M., Banerjee, S., Yadigaroglu, G., 2008. Turbulence and heat transfer in condensing vapor-liquid flow. Phys. Fluids 20, 065101.

Lakehal, D., Labois, M., 2011. A new modelling strategy for phase-change heat transfer in turbulent interfacial two-phase flow. Int. J. Multiph. Flow 37 (6), 627–639.

Lakehal, D., Liovic, P., 2011. Turbulent structure and interaction with steep breaking waves. J. Fluid Mech. 674, 522–577.

Lakehal, D., Metrailler, D., Reboux, S., 2017. Turbulent water flow in a channel at re $\tau=$ 400 laden with 0.25 mm diameter air-bubbles clustered near the wall. Phys. Fluids 29 (6), 065101.

Lakehal, D., Smith, B., Milelli, M., 2002. Large-eddy simulation of bubbly turbulent shear flows. J. Turbul. 3(25), 1–21.

Lance, M., Marie, J., Charnay, G., Bataille, J., 1979. Turbulence in Bubbly Blow: From Experiments to Numerical Modelling, t. 288. Comptes Rendus de l'Acadmie des Sciences - Series A, pp. 957–960.

Landau, L., Lifshitz, E., 1987. Fluid Mechanics, second ed. Pergamon Press.

Li, S., Wang, P., Lu, T., 2015. Numerical simulation of direct contact condensation of subsonic steam injected in a water pool using vof method and les turbulence model. Prog. Nucl. Energy 78, 201–215.

Liovic, P., Lakehal, D., 2006. Interface-turbulence interactions in large-scale bubbling processes. Int. J. Heat Fluid Flow 28, 127–144.

Liovic, P., Lakehal, D., 2007. Multi-physics treatment in the vicinity of arbitrarily deformable gas-liquid interfaces. J. Comput. Phys. 222, 504–535.

Liovic, P., Lakehal, D., 2012. Subgrid-scale modelling of surface tension within interface tracking-based large eddy and interface simulation of 3d interfacial flows. Comput. Fluids 63.

Ma, T., Ziegenhein, T., Lucas, D., Fröhlich, J., 2016. Large eddy simulations of the gas–liquid flow in a rectangular bubble column. Nucl. Eng. Des. 299, 146–153.

Mason, P., Thomson, D., 1992. Stochastic backscatter in the large-eddy simulations of boundary layers. J. Fluid Mech. 242, 51–78.

Metrailler, D., Reboux, S., Caviezel, D., Lakehal, D., 2015. Dns of turbulent convective flow boiling in a channel. In: Proceedings of the NURETH-16. ANS, Chicago, USA.

Milelli, M., Smith, B., Lakehal, D., 2001. Large-eddy simulation of turbulent shear flows laden with bubbles. Direct and Large-Eddy Simulation IV.

Navarro-Martinez, S., 2014. Large eddy simulation of spray atomization with a probability density function method. Int. J. Multiph. Flow 63, 11–22.

Ničeno, B., Dhotre, M., Deen, N., 2008. One-equation sub-grid scale (SGS) modelling for euler–euler large eddy simulation (EELES) of dispersed bubbly flow. Chem. Eng. Sci. 63 (15), 3923–3931.

Osher, S., Sethian, J.A., 1988. Fronts propagation with curvature–dependent speed: algorithm based on hamilton–jacobi formulations. J. Comp. Phys. 79, 12.

Piquet, J., 2013. Turbulent Flows: Models and Physics. Springer Science & Business Media.

Prosperetti, A., Zhang, D., 1994. Ensemble phase-averaged equations for bubbly flows. Phys. Fluids 8, 2956–2970.

Reboux, S., Sagaut, P., Lakehal, D., 2006. Large-eddy simulation of sheared interfacial flow. Phys. Fluids 18(10), 105105.

Sato, Y., Sadatomi, M., Sekoguchi, K., 1981. Momentum and heat transfer in two-phase bubble flowi. theory. Int. J. Multiph. Flow 7 (2), 167–177.

Scardovelli, R., Zaleski, S., 1999. Direct numerical simulation of free-surface and interfacial flow. Ann. Rev. Fluid Mech. 31, 567.

Shinjo, J., Umemura, A., 2010. Simulation of liquid jet primary breakup: dynamics of ligament and droplet formation. Int. J. Multiph. Flow 36 (7), 513–532.

Simiano, M., Lakehal, D., Lance, M., Yadigaroglu, G., 2009. Turbulent transport mechanisms in oscillating bubble plumes. J. Fluid Mech. 633, 191–231.

Sirignano, W., 2005. Volume averaging for the analysis of turbulent spray flows. Int. J. Multiph. Flow 31, 675–705.

Sirignano, W.A., 1999. Fluid Dynamics and Transport of Droplets and Sprays. Cambridge University Press.

Slattery, J., 1967. Flow of viscoelastic fluids through porous media. AIChE J. 13, 1066–1071.

Smagorinsky, J., 1963. General circulation experiments with the primitive equations i the basic experiment. Mon. Weather Rev. 91, 99–165.

Sussman, M., Fatemi, E., Smereka, P., Osher, S., 1998. Improved level set method for incompressible two-phase flows. Comput. Fluids 27, 663–680.

Tabib, M.V., Schwarz, P., 2011. Quantifying sub-grid scale (SGS) turbulent dispersion force and its effect using one-equation sgs large eddy simulation (LES) model in a gas–liquid and a liquid–liquid system. Chem. Eng. Sci. 66 (14), 3071–3086.

Toutant, A., Chandesris, M., Jamet, D., Lebaigue, O., 2009. Jump conditions for filtered quantities at an under-resolved discontinuous interface. part 2: a priori tests. Multiph. Flow 35, 1100–1118..

Tran, M., 2000. Modélisation Instationnaire de la Distribution Spatiale des Phases dans LES Ecoulements Diphasiques en Régimes à Bulles. Doctoral Thesis, University of Claude Bernard, Lyon.

Unverdi, S., Tryggvason, G., 1992. A front-tracking method for viscous, incompressible, multi-fluid flows. J. Comput. Phys. 100, 25.

Vaidheeswaran, A., Hibiki, T., 2017. Bubble-induced turbulence modeling for vertical bubbly flows. Int. J. Heat Mass Transf. 115, 741–752.

Vincent, S., Lacanette, D., Larocque, J., Toutant, A., Lubin, P., Sagaut, P., 2008. Direct numerical simulation of phase separation and *a priori* two-phase LES filtering. Comput. Fluids 37, 898–906.

Whitaker, S., 1966. The equations of motion in porous media. Chem. Eng. Sci. 21, 291–300.

Whitaker, S., 1967. Diffusion and dispersion in porous media. AIChE J. 13, 420–427.

Williams, F., 1962. Detonations in Dilute Sprays. In: Detonation and Two-Phase Flow. Elsevier, pp. 99–114.

Yang, D., Chen, B., Socolofsky, S.A., Chamecki, M., Meneveau, C., 2016. Large-eddy simulation and parameterization of buoyant plume dynamics in stratified flow. J. Fluid Mech. 794, 798–833.

Zhang, D.Z., Prosperetti, A., 1997. Momentum and energy equations for disperse two-phase flow and their closure for dilute suspensions. Int. J. Multiph. Flow 23, 425–453.